Magnetic phase transitions

in superconducting vanadium

by

Kathleen Weland Haas

An Abstract of

A Thesis Submitted to the

Graduate Faculty in Partial Fulfillment of

The Requirements for the Degree of

MASTER OF SCIENCE

Approved:

_____

In Charge of Major Work

_____

For the Major Department

_____

For the Graduate College

Iowa State University
Ames, Iowa

1973

Magnetic phase transitions in superconducting vanadium*

Kathleen Weland Haas

Under the supervision of D. K. Finnemore
From the Department of Physics
Iowa State University

The magnetization of very pure vanadium ($\rho_{300\ K}/\rho_{4.2\ K} = 1500$) has been measured for reduced temperatures between 0.225 and 0.958 in order to study the nature of the phase transition at the lower critical field for this low-κ ($\kappa = 0.82$), long mean free path ($\ell \approx 60\ \xi_o$) material. The transition was analyzed to determine the equilibrium flux density, B_o, and the equilibrium flux-line lattice parameter, d_o, at initial flux penetration. The flux-line lattice parameter was found to agree well with the expression $d_o(t) = (1.73 \pm 0.1) \times 10^3\ \text{Å}\ (1 - t)^{-\frac{1}{2}}$. Critical field curves and generalized Ginzburg-Landau parameters were found to be in good agreement with earlier work by Sekula and Kernohan on less pure samples.

---

*USAEC Report IS-T-585. This work was performed under Contract W-7405-eng-82 with the Atomic Energy Commision.

Magnetic phase transitions in superconducting vanadium

by

Kathleen Weland Haas

A Thesis Submitted to the
Graduate Faculty in Partial Fulfillment of
The Requirements for the Degree of
MASTER OF SCIENCE

Department: Physics

Major: Solid State Physics

Approved:

_____
In Charge of Major Work

_____
For the Major Department

_____
For the Graduate College

Iowa State University
Ames, Iowa

1973

TABLE OF CONTENTS

INTRODUCTION

For the past several years, there has been a controversy in the literature concerning the nature of the phase transition in a type-II superconductor at the field, called H_{c1}, for which magnetic flux first begins to penetrate the sample. Early theoretical work indicated that one might expect a second-order transition at H_{c1}, and indeed this seems to be the case for one class of type-II materials. Recent work however on the elemental type-II superconductors has indicated that perhaps they show a first-order transition at H_{c1}. This study of the magnetization of pure vanadium has been undertaken to provide more evidence concerning the phase transition in the elemental type-II materials at H_{c1}.

Theoretical Background

The response of a superconductor to an applied magnetic field depends on the penetration depth, λ, the coherence length, ξ, and the normal state mean free path, ℓ. In the theory, magnetic behavior is discussed in terms of the Ginzburg-Landau (1) parameter κ, which is proportional (2) to the ratio λ/ξ. For most pure elements, ℓ and ξ are both much greater than λ, hence κ is small, and the material exhibits type-I behavior (3) as illustrated in Figure 1a. At sufficiently low fields, type-I materials exhibit a complete Meissner effect; that is, all magnetic flux is completely excluded from the bulk of the sample. As the field is increased to a value H_c, an ideal infinitely long, thin sample of type-I material will abruptly become normal, thus allowing complete magnetic flux penetration.

For many so-called "dirty" materials, such as solid solution alloys, ℓ and ξ are much smaller than λ so $\kappa \gg 1$, and the material exhibits extreme type-II behavior (4) as illustrated in Figure 1b. A long thin sample of type-II material exhibits a complete Meissner effect at low fields but will not undergo a complete transition to the normal state at the field, called H_{c1}, at which magnetic flux initially penetrates the sample. Rather it will remain superconducting and exhibit a partial Meissner effect over a fairly wide range of field above H_{c1}. The field at which flux penetration is complete and the bulk of the sample is normal is called H_{c2}. When $H_{c1} \leq H \leq H_{c2}$, the sample is said to be in the mixed, vortex, or Shubnikov state.

The transition from the Meissner to the normal state in type-I materials and the transition from the Meissner to the vortex state in extreme type-II materials are fairly well understood. In type-I materials the transition is first-order (5), while in extreme type-II materials it is second order (6). There exist some pure elements and alloys however for which $\xi \approx \lambda$, or $\kappa \approx 1$, and this case is less well understood. These materials are classified as type-II because they show a vortex state, but they do not show a second-order transition at H_{c1}, rather they undergo a first-order transition. These materials are referred to as low-κ type-II superconductors. The first-order transition which they show at H_{c1} reflects the fact that the forces between the vortices are attractive rather than repulsive as in the high-κ type-II materials.

Initially, theory favored the repulsive interaction for all type-II materials. Abrikosov's (6) solution to the Ginzburg-Landau equations

predicted a second-order transition at H_{c1} and Goodman (7) pointed out that Abrikosov's treatment led to a λ-type second-order transition. Meanwhile McConville and Serin (8,9,10) measured the specific heat of niobium, a low-κ type-II material, and found what appeared to be a first-order transition. Later Serin (11) measured the magnetization of niobium and concluded that the transition was instead a second-order λ-type transition in agreement with Goodman's prediction.

The work of Krägeloh (12,13) and that of Träuble and Essmann (14) soon challenged the theory. They observed flux-line patterns in low-κ type-II materials using a modified Bitter decoration technique and found that a lattice of fluxoids can exist adjacent to a region which is in the Meissner state. This suggests that the fluxoids attract one another. Hence the magnetic phase transition at H_{c1} should be first-order. At this writing, no consensus exists as to the correct theoretical justification for this attractive interaction, though a number of possible explanations have appeared in the literature (15-25).

Experimental Background

Three types of experimental evidence for the attractive interaction between fluxoids are now available. The first, and strongest, type of evidence is the previously mentioned fluxoid patterns obtained by Essmann and Träuble's decoration technique (12-14,26-30). The second type of evidence comes from neutron diffraction studies (31,32,33) which show the structure not only of the fluxoid lattice but also of the individual vortices. Finally, the third type of evidence is an indication of a first-order transition in the magnetization curve at H_{c1} (34-37). Experi-

mentally this is difficult to establish because of demagnetization and pinning effects which tend to broaden the transition.

Essmann (29) has pointed out that an attractive interaction between flux lines would give rise to the magnetization curves shown in Figure 2 for low-κ type-II superconductors. The long range attractive interaction between fluxoids does not allow one fluxoid alone to penetrate an ideal specimen whose demagnetizing factor, D, is zero. Rather the first fluxoid is immediately joined by many others until the entire sample is filled with a "crystal" of fluxoids. This "crystal" of fluxoids will have a lattice parameter d_o, where d_o is the most energetically favorable distance between two vortices.

When the fluxoid crystal has grown until it reaches the edge of the sample, it suddenly becomes much less favorable for new fluxoids to penetrate the specimen. It is clear that the size of the lattice parameter, d_o, determines how many fluxoids will be able to occupy the sample. That, in turn, determines the average magnetic induction, B_o, in the sample. For the most common case of a triangular flux-line lattice

$$B_o = \frac{2\varphi_o}{\sqrt{3}\, d_o^2} , \qquad (1)$$

where φ_o is the flux quantum. We see then that the magnetization of the specimen changes abruptly by an amount $B_o/4\pi$ at H_{c1}. As the field is increased above H_{c1}, each new fluxoid must crowd the existing ones closer together than the most energetically favorable distance, causing distortion in the fluxoid lattice. Since it is now harder for each flux line to force its way into the sample, the magnetization changes less rapidly as the field is further increased.

Seeger (38) has given an excellent explanation of the complications which arise due to the non-zero demagnetizing factor. In a type-I superconductor, $D \neq 0$ gives rise to the well known intermediate state, while in low-κ type-II superconductors one sees a so-called intermediate mixed state. This intermediate mixed state arises only when the long range attractive interaction between fluxoids is present, that is, for $\kappa \approx 1$. It provides a transition region from the pure Meissner state to the pure mixed state when $D \neq 0$. The type of flux density associated with the intermediate, the intermediate mixed, and the pure mixed states are shown in Figure 3.

The existence of the intermediate mixed state leads to a linear region in the magnetization curve just above H_{c1} as shown in Figure 2b. The purpose of this work is to seek that type of magnetization curve for very pure vanadium. Such curves allow us to calculate B_o and d_o as a function of temperature. We also obtain critical field curves and values of the generalized Ginzburg-Landau parameters, κ_1 and κ_2. The magnetization of vanadium has been measured previously by Sekula and Kernohan (39) and Radebaugh and Keesom (40) but their samples were less pure, having resistivity ratios, $\rho_{300\ K}/\rho_{4.2\ K}$, three and ten times smaller respectively than that of the sample used here.

EXPERIMENTAL DETAILS

Sample

The sample was a long cylindrical vanadium rod which was prepared by F. A. Schmidt of this laboratory from fused-salt electrofined vanadium by the electrotransport technique described in Reference 41. The resistivity ratio ($\rho_{300\ K}/\rho_{4.2\ K}$) was determined by J. E. Ostenson of this laboratory to be 1500. Before the magnetization measurements were made the ends of the sample were ground to roughly hemispherical shape and the specimen was electropolished in a 6% perchloric acid in methanol solution at -70°C to the final dimensions of 1.002 inches long and 0.091 inch in diameter. The transition temperature was determined by an ac susceptibility measurement to be 5.43 ± 0.02 K by J. E. Ostenson. The demagnetizing factor of this sample was taken to be 0.0175 which is the value tabulated by Stoner (42) for an ellipsoid of revolution with the same length to diameter ratio as this rod.

The rod contained a number of grains which extended across the entire diameter of the sample, the largest of which was about 0.19 inch long. This grain, which was located near the center of the rod, was centered in the 0.25 inch long pick-up coil for all magnetization runs, so the magnetization data primarily reflect the behavior of this grain. The orientation of this largest grain was determined by O. D. McMasters of this laboratory using a Laue back-reflection camera. The [110] crystal axis was found to lie along the axis of the rod. The orientation of the grains on either side of the largest one were also determined and each was found to have a ⟨110⟩ crystal axis within seven degrees of the axis of the rod.

After most of the data had been taken, the sample was further electropolished until it very roughly resembled an ellipsoid of length 0.816 inch, major diameter 0.044 inch, and minor diameter 0.032 inch. One final set of data was then taken to determine the effects of sample geometry on the shape of the curve. The grain boundaries were no longer visible on this reduced sample, so the sample as a whole was centered in the pick-up coil. The demagnetizing factor for the reduced sample was approximated by Stoner's (42) value for an ellipsoid of revolution with a length 0.816 inch and diameter 0.032 inch. That value was D = 0.005.

Cryostat

Magnetization measurements were made using the sample-motion magnetometer shown in Figure 4. The sample was placed in a movable copper sample holder which in turn was in a 0.25 inch long coil of 16,300 turns of No. 44 copper wire. In order to buck out any signal caused by variations in the external field, a similar oppositely wound coil was placed in series with the pick-up coil.

Because the distance the sample moved was fairly large, it was necessary to have a magnetic field that was homogeneous over a substantial region. To produce this field, a liquid nitrogen cooled solenoid was placed around the outer wall of the liquid helium dewar. The solenoid was constructed from No. 14, square, pure-annealed copper wire with teflon spacers to allow circulation of liquid nitrogen. Additional layers of windings were placed on each end of the solenoid to provide a more uniform field near its center. The magnitude of the field produced by the solenoid as a function of the current through the solenoid was known from J. R.

Hopkins' calibration to be 152.45 ± 0.02 Oe/A. He found that the field was homogeneous to within 0.3% over a volume of six cubic inches near the center of the solenoid. The sample and pick-up coil were placed within that homogeneous region. The counterwound coil in series with the pick-up coil was placed in a region which Hopkins' measurements showed to be within 0.4% of the field at the center of the solenoid. For this work, it was verified, using a Bell 240 Incremental Gaussmeter, that the field was homogeneous to within 0.3% over the entire length of the sample and over its entire length of travel.

The temperatures were measured using a standard four terminal germanium resistance thermometer, Honeywell 251. The precision in this experiment was ±0.001 K but the accuracy was limited by the calibration to ±0.010 K. This thermometer had been calibrated by Finnemore against constant volume gas thermometry. These data were fit to the polynomial

$$\ln T = \sum_{n=0}^{7} A(n) \left[\ln(R/R_o)\right]^n$$

in several overlapping ranges of temperature. The coefficients and their range of validity are listed in Appendix I. The thermometer was placed in a phenolic holder in the coil form just above the pick-up coil.

A major problem when making measurements directly in a liquid helium bath is that the relatively poor thermal conductivity of the helium permits temperature gradients as large as several millikelvin to develop in the experimental region. To help alleviate this problem, this system was designed with a copper heat shield extending from the top of the coil form to within 0.5 inch of the bottom of the liquid helium dewar. The

temperature of this shield was controlled by a heater consisting of a coil of No. 36 manganin wire wound around the lower edge of the heat shield. A sensing thermometer was mounted in a copper collar which, in turn, was soldered just inside the lower edge of the heat shield. This thermometer was intended to be used to help control temperature but turned out not to be necessary.

Sample-lifting Device

If the sample is to remain at constant temperature during the entire run, it must be extracted from the pick-up coil as smoothly as possible to minimize heating caused by mechanical vibrations. It must also be extracted rapidly so that the voltage pulse produced in the pick-up coil occurs in a very short time compared to the period of the galvanometer, which in this case was 9.3 seconds. The device developed to provide the necessary smooth but rapid sample motion is shown in Figure 5. Brass bellows, mounted on the top plate of the cryostat, were alternately evacuated and pressurized through a solenoid operated valve. Because the top of the bellows was held fixed, evacuating them caused the bottom of the bellows to move upward. This motion was transmitted to the sample by a long stainless steel tube used as a pushrod, thus extracting the sample from the pick-up coil. High pressure air was used to return the bellows, and thus the sample, to their original position. The device was designed so that the initial and final positions of the sample could be chosen independently and could be as much as 1.5 inches apart. This allowed various parts of the sample to be centered in the 0.25 inch long pick-up coil.

Electronics

The magnetization of the sample was determined from the voltage pulse generated in a pick-up coil when the sample was abruptly removed from the coil. This pulse was measured ballistically by a Leeds and Northrup No. 2285X Galvanometer with period 9.3 seconds and critical damping resistance 1050 ohms. A decade resistor placed in parallel with the pick-up coil provided a shunt so that the signal remained within the scale of the galvanometer. Another decade resistor was placed in series with the coil and galvanometer to provide the critical damping resistance. The galvanometer deflection was read on a Leeds and Northrup No. 2100 Lamp and Scale Reading Device placed 206 cm from the galvanometer mirror.

The external magnetic field was provided by a liquid nitrogen cooled solenoid, which as discussed previously, was known to provide a field of 152.45 ± 0.02 Oe/A. The current for the solenoid was provided by a Spectromagnetic Current Regulated Power Supply capable of putting up to 50 amperes through a one ohm load with a stability of $\pm 1 \times 10^{-5}$ over eight hours. The solenoid current was measured by determining the voltage drop across a Rubicon 0.01 ohm, 100 ampere resistor placed in series with the solenoid. That voltage was measured by a Keithley Instruments Model 662 Guarded DC Differential Voltmeter.

The germanium resistor, Honeywell 251, carried a 10 microampere current provided by mercury cells. The voltage drop across this resistor was measured by a standard four probe dc technique using a Leeds and Northrup Type K-3 Potentiometer and a Keithley Instruments Model 150B Microvolt Ammeter.

Temperature Control

In order to insure that the temperature of the sample remained constant, all measurements were made with the sample in the liquid helium bath. The temperature was established by regulating the pressure over the bath. In order to minimize temperature gradients within the bath, the heater was used to provide stirring.

The pressure over the bath was regulated in several ways. For the lowest temperatures, 1.22 K and 1.93 K, the pressure was controlled manually by adjusting the pumping rate through a valve. For other temperatures below 4.2 K a manostat was used in the pumping line to maintain the desired pressure. At 4.20 K, the bath was simply exhausted to the atmosphere. In all of the above cases, ten milliwatts of heat were used to stir the bath. For temperatures above 4.20 K the manostat was again used but was exhausted to atmospheric pressure rather than to the pump. At these higher temperatures, as much as 400 milliwatts of power were used initially to bring the bath up to temperature. When the temperature had stablized, the heater power was cut back to between ten and one hundred milliwatts to provide stirring while data were being taken.

The temperature was controlled to ±0.001 K for Runs 11, 12, 16, 20, 21, 23, and 25; to ±0.002 K for Runs 14 and 26; and to ±0.005 K for Runs 18 and 19. For Run 17, the temperature was controlled to ±0.001 K except during the time the last nine data points were taken when it rose 0.010 K.

RESULTS

Magnetization Curves

The results of the magnetization measurements are shown in Figures 6 through 9. In the Meissner region

$$B = H + 4\pi M = 0,$$

hence

$$H = -4\pi M.$$

This means the magnetization curves, plotted as $-4\pi M$ versus H, show a straight line whose slope equals plus one as long as the field is low enough to allow the sample to remain completely in the Meissner state. When H reaches H_{c1}, flux begins to penetrate the sample, hence the magnetization curve begins to drop away from the Meissner line. The magnetization drops to zero at H_{c2}, at which point the sample is normal except for a thin surface sheath.

The absolute value of the magnetization was obtained from the galvanometer deflection by assuming that the slope of $-4\pi M$ versus H_a, the applied field, in the Meissner region was $1/(1 - D)$, where D is the demagnetizing factor of the sample (43). The values of H shown in Figures 6 through 9 have been corrected for demagnetizing effects according to

$$H = H_a - 4\pi MD, \qquad (2)$$

where H_a is the applied field (38). The effect of this correction on the shape of the curve in the vicinity of H_{c1} is demonstrated in Figure 10, where the data are shown both as a function of the applied field, H_a, and the corrected field, H. This shows that the correction in equation (2) brings the slope of the curve down from $1/(1 - D)$ to one and causes the

drop in magnetization at H_{c1} to appear steeper.

The corrections mentioned above are useful only to the extent that the sample can be characterized by one constant value of D. In practice, D will be the same for all points in the sample only if the sample is a homogeneous ellipsoid. The values of D for homogeneous ellipsoids of revolution with the external field parallel to the axis of revolution have been tabulated by Stoner (42). For this experiment, the sample was a long, thin rod with the ends ground to roughly hemispherical shape. This shape is reasonably close to an ellipsoid of revolution so Stoner's value of D for an ellipsoid of revolution with the same length to diameter ratio as the rod was used. That value was D = 0.0175. It must also be noted that the sample was not truly homogeneous, because it did consist of several grains which had slightly different crystal orientations.

Near H_{c1} the shape of the curve is very sensitive to the value of the demagnetizing factor, as shown in Figure 2a and 2b. In an ideal sample with no flux pinning effects, uniform demagnetizing factor, applied field parallel to the axis of the sample, and magnetization parallel to the applied field, one expects the slope of the magnetization curve just above H_{c1} to be -1/D before the correction in equation (2) is made, and minus infinity after the correction. In this work, the sample shows a slope of $-1/(3.2\ ^{+\ 1.5}_{-\ 0.8})D$ before correction and $-1/(2.1\ ^{+\ 1.5}_{-\ 0.8})D$ afterwards. This reflects the fact that the sample is not ideal.

There are several reasons why the sample might not show ideal behavior. As mentioned before, the sample is not entirely homogeneous, nor is it an exact ellipsoid. In addition, it probably shows both bulk

and surface pinning effects, and it may have some anisotropy which causes the flux lines to lie along a certain preferred crystal axis, even if that axis is not parallel to the external field. This latter effect has been seen by neutron diffraction in niobium (32,33), where the preferred axis was the ⟨111⟩, but there is no corresponding data for vanadium. Decoration experiments by Lishke and Rodewald (44) on vanadium have shown that the flux-line lattice is somewhat anisotropic in that it forms triangles with angles of 62, 54, and 64 degrees, but similar work by Essmann (30) on vanadium has shown no correlation between flux-line lattice and crystal lattice. It should also be noted that neither Lishke and Rodewald nor Essmann observed an intermediate mixed state in vanadium. As yet no one has reported which crystal axis, if any, is a preferred direction for flux lines in vanadium, so one cannot ascribe the finite slope of the magnetization curve at H_{c1} to this effect with any certainty. Finally, the shape of the magnetization curves near H_{c1} would be very sensitive to temperature drifts. If the temperature were rising slowly, the slope of the magnetization curve just above H_{c1} would become slightly steeper; if it were falling, the slope would tend to flatten out somewhat. Such drifts should have been no larger than two millikelvin during the transition for any run, so the effects should be minimal.

If the demagnetizing factor used for this sample is inaccurate, it probably errs by being too low. If a larger value, D', were chosen, there would be two effects on the curves shown. First, the values of $-4\pi M$ would all be increased by the factor $(1 - D)/(1 - D')$. This would result from recalibrating the galvanometer deflections so that the slope of $-4\pi M$

versus H_a in the Meissner region would be $1/(1 - D')$. Second, the transition at H_{c1} would appear steeper than it does for the curves shown because of equation (2).

The fact that the $-4\pi M$ versus H_a curves show an average slope of $-1/3.2$ D, rather than $-1/D$, just above H_{c1} suggests that the effective demagnetizing factor for this sample is no larger than 3.2 D. If we replace D by $D' = 3.2$ D, the values of M would rise by 4%. That number represents a limit on the accuracy of M. Because M and H are related by equation (2), the accuracy of H is limited by the accuracy of M except when M equals zero.

In order to test the effect of sample geometry on the shape of the magnetization curves, the sample was electropolished down to a smaller diameter and another set of data were taken. Unfortunately, the sample did not remain cylindrical during electropolishing, so it was difficult to assign a value for its demagnetizing factor. To avoid the possibility of causing the transition region to appear steeper than it ought to, the demagnetizing factor was deliberately chosen to be as low as possible. This was done by using Stoner's (42) value for the demagnetizing factor of an ellipsoid of revolution whose diameter equaled the minimum diameter of the reduced sample. That value was $D = 0.005$.

Data taken on the reduced sample at $T = 4.18$ K are compared with data taken on the original sample at $T = 4.20$ K in Figure 11. The overall agreement between the curves is excellent, but there are small deviations near H_{c1}. Figures 12 and 13 show the magnetization curves near H_{c1} in more detail. In Figure 12, the magnetization is plotted as a function of

applied field, H_a, while in Figure 13 it is shown as a function of the field H defined in equation (2). The transition is seen to be steeper in the reduced sample than in the original sample; and it occurs at a slightly higher field as was expected for the data taken at a slightly lower temperature. The amount of shift in the curves expected due to the difference in temperature between the runs is indicated on each figure. In the curves which have been corrected for demagnetizing effects, the observed shift is inexplicably smaller than the predicted shift. A similar prediction was made for the shift in the upper critical field; and the observed shift agreed to within 5%. This suggests that the shape of the curve near H_{c1} is more dependent on sample geometry than it is near H_{c2}.

The Transition at the Lower Critical Field

In order to determine whether the transition from the Meissner to the mixed state was first-order or second-order, it was necessary to take a detailed look at the slope of the magnetization curve near H_{c1}. First, the slope between each pair of points, $-4\pi\Delta M/\Delta H$, was calculated, then $-4\pi M$ was plotted as a function of $-4\pi\Delta M/\Delta H$. This somewhat unusual presentation allows one to see how much of the drop in magnetization takes place in the region where the slope is the steepest. If the transition is first-order, one expects $-4\pi M$ versus $-4\pi\Delta M/\Delta H_a$ to look like Figure 14a; if the transition is second-order, one expects Figure 14b. A typical curve obtained for the original sample is shown in Figure 15 and the curve for the reduced sample in Figure 16. Curves taken at all temperatures were very similar. It should be noted that these curves are based on data

which has been corrected for the theoretical value of D, so if the sample were ideal, these curves would show D = 0 behavior.

Because the minimum slope observed near H_{c1} is predicted to be -1/D for both first-order and λ-type second-order transitions, a sample with D = 0 would have a minimum slope of minus infinity. The minimum slope actually observed in each run gives an indication of what might be called the residual demagnetizing factor; that is, this number gives some measure of the non-ideality of the sample. The minimum slope observed in five of the eleven runs taken with the original sample was between -25.6 and -28.6, and averaged -27.2 = -1/2.10 D. For all eleven runs it was between -15.8 and -42.5 and averaged -27.4 = -1/2.08 D. For the reduced sample the minimum slope was -36.2 = -1/5.52 D. The fact that almost half of the runs show a very similar minimum slope indicates that the slope is characteristic of the individual sample, perhaps a function of its geometry, orientation in the field, surface and bulk pinning properties.

The shape of the $-4\pi M$ versus $-4\pi\Delta M/\Delta H$ curves obtained in this work does not provide conclusive evidence whether the transition is first- or second-order. The curves do not show the sharp drop in $-4\pi M$ expected for a first-order transition although they do show a drop which might be regarded as a rounded version of the first-order drop. Such rounding could be explained by one or more of the effects discussed earlier, namely bulk or surface pinning, a non-uniform demagnetizing factor in the sample, preferential alignment of the flux lines along a crystal axis not parallel to the applied field, or a slight temperature drift while data were being taken.

Calculation of B_o and d_o

Because the experimental work of Auer and Ullmaier (37) and the theoretical work of Leung and Jacobs (25) indicate that a first-order transition should be expected, an attempt was made to analyze the data under this assumption thus obtaining the parameters B_o, the equilibrium flux density, and d_o, the equilibrium flux-line lattice parameter at initial flux penetration. From Figure 2a, we see that

$$B_o = H_{kink} + 4\pi M_{kink} \tag{3}$$

where H_{kink} and $-4\pi M_{kink}$ are the coordinates of the point at which the sharp drop in magnetization terminates. Because there is no clear cut kink in this data, it was decided to define the kink to be at the point on the magnetization curve at which the slope of the curve reached a certain value, namely $(-4\pi\Delta M/\Delta H)_{kink} = -12.0$. In the ideal case there would be a discontinuity in the slope at the kink. Because that does not occur in this data, we chose instead to assume that the kink occurred in the region where the magnetization curve began to flatten out so that it dropped less steeply toward zero. In order to choose $(-4\pi\Delta M/\Delta H)_{kink}$, each magnetization curve was studied to determine visually where the kink seemed most likely to be, then the value of $-4\pi\Delta M/\Delta H$ at that point was determined and recorded. After this had been done for all the magnetization curves, the average value of $-4\pi\Delta M/\Delta H$ at the apparent kinks was found, and defined to be $(-4\pi\Delta M/\Delta H)_{kink}$. As mentioned above, that value was $(-4\pi\Delta M/\Delta H)_{kink} = -12.0$. It is interesting to note that this is fairly close to half the value of the maximum slope observed for most runs. Using this criterion, the value of $-4\pi M_{kink}$ could be read off the $-4\pi M$ versus $-4\pi\Delta M/\Delta H$ curves

for each run. Then using this value of $-4\pi M_{kink}$ and the magnetization curves, one could determine the value of H_{kink}. B_o could then be determined using equation (3). The values of H_{kink}, $-4\pi M_{kink}$, and B_o as a function of reduced temperature, $t = T/T_c$, are shown in Figure 17. In Figure 18, the same quantities are shown as a function of t^2, and we notice that H_{kink} shows fairly good correspondence to $1 - t^2$ behavior but $-4\pi M_{kink}$ and B_o do not.

The equilibrium flux line parameter, d_o, can be calculated from

$$d_o = \sqrt{\frac{2\,\varphi_o}{\sqrt{3}\,B_o}},$$

where $\varphi_o = hc/2e = 2.07 \times 10^{-7}$ gauss-cm^2 is the flux quantum. The values obtained for d_o as a function of t are shown in Figure 19. The temperature dependence of d_o is still the subject of theoretical investigation but preliminary work (20) seems to indicate that d_o should have the same temperature dependence as the penetration depth, λ. Hence the data are compared with a curve of the form

$$d_o(t) = d_o(0) \,/\, \sqrt{1 - t}$$

where $d_o(0)$ was determined from the experimental points to be $d_o = (1.73 \pm 0.1) \times 10^3$ Å. This curve, shown in Figure 19, fits the data to within 1% for five of the data points, within 2.8% for an additional four points, and within 5.7% for the remaining two points.

The flux-line lattice parameter of vanadium in the mixed state has been determined by Lishke and Rodewald (44) using a decoration technique. They found a slightly anisotropic triangular flux-line lattice with d_{min} =

2600 Å and d_{max} = 2700 Å at T = 1.2 K, H_a = 200 Oe for a thin vanadium slab with demagnetizing factor D = 0.8 and κ(1.2 K) = 3.2. This is 30% higher than the value obtained in this work for a long cylindrical sample with κ(1.2 K) = 1.2. One expects d_o to be smaller for a purer sample, that is, one with a lower κ, so the agreement between the two experiments is rather good.

So far, no value has been given for H_{c1}. In Figure 2a it can be seen that H_{c1} is the field at which a discontinuous drop in $-4\pi M$ occurs. Because no such drop is observed in this data, even when it has been corrected nominally to D = 0, no attempt has been made to define H_{c1}. The value of H_{kink} defined above however closely approximates H_{c1}.

The Upper Critical Field

The upper critical field, H_{c2}, is defined as the point at which the magnetization curve reaches zero as shown in Figures 1 and 2. The values of H_{c2}, obtained to a precision of ± 3% in this work, are shown in Figure 20. These values lie within 2% of those found by Sekula and Kernohan (39) for $t < 0.8$ and within 4% for $t > 0.8$. In order to make a direct comparison of the temperature dependence of H_{c2} with theory, one calculates the quantity $h^*(t)$ which was introduced by Helfand and Werthamer (45) and is defined by

$$h^*(t) = H_{c2}(t) \; / \; \left|dH_{c2}/dt\right|_{t=1} .$$

For this work $\left|dH_{c2}/dt\right|_{t=1} = (3.33 \pm 0.2) \times 10^3$ Oe. A plot of $h^*(t)$ versus t, shown in Figure 21 along with the theoretical curve predicted by Helfand and Werthamer (45), indicates that the data lie somewhat higher than the theoretical curve. The data point at the lowest temperature,

$t = 0.225$, deviates the most, lying 11% above the theoretical curve. Sekula and Kernohan's data lie even higher, deviating from the theory by 24% at $t = 0.225$. Their deviations are greater because they found $\left|dH_{c2}/dt\right|_{t=1} = (3.03 \pm 0.12) \times 10^3$ Oe which is 9% lower than the value obtained for this work. This is probably not too significant, since the precision with which this value has been determined is only about ± 5%.

The Thermodynamic Critical Field

The thermodynamic critical field, $H_c(t)$, can be calculated from the area under the magnetization curve according to

$$H_c^2 = 2 \int_0^{H_{c2}} (-4\pi M)\, dH \,. \qquad (4)$$

The resulting critical field curve is shown in Figure 20 and the deviation of these values from $1 - t^2$ behavior is shown in Figure 22. The deviation predicted by BCS theory is also shown. The shape of the deviation suggests that perhaps T_c was larger than the value $T_c = 5.43$ K used here by nearly 0.050 K. The deviations were recalculated using $T_c = 5.48$ K and these values are also shown. Using the higher value of T_c makes the curve more symmetrical but results in larger deviations from $1 - t^2$ behavior and from BCS behavior. The accuracy of H_c is proportional to the accuracy of the calibration of M, which as discussed earlier is limited by the uncertainty in the value of the demagnetizing factor D. Fetter and Hohenberg (46) have shown that the value obtained for H_c is independent of whether the integral in equation (4) is taken over H or H_a, so that any inaccuracy in H due to the uncertainty of D does not effect H_c. Again, it

is only the uncertainty in M itself which appears. The critical fields measured in this work are in good agreement with those measured by Sekula and Kernohan (39). Values reported here are about 3% higher than Sekula's for t greater than 0.3 and rise to 5% higher at t = 0. Sekula and Kernohan obtained $H_c(0) = 1408 \pm 35$ Oe; the value obtained in this work is $1480 \begin{smallmatrix} + 60 \\ - 0 \end{smallmatrix}$ Oe.

All data shown in Figures 6 through 13 were taken as H_a, the applied field, was increased. Data taken on the original sample as H_a was decreased showed significant hysteresis and trapped flux as shown in Figure 23. Data taken on the reduced sample are shown in Figure 24. The trapped flux in the original sample gave

$$-4\pi M(H_a=0) = -13.9 \pm 0.2 \text{ gauss},$$

whereas for the reduced sample

$$-4\pi M(H_a=0) = +0.3 \pm 0.3 \text{ gauss}.$$

To compare reversibility, the thermodynamic critical field was calculated using the decreasing field curve, and compared to the value obtained using the increasing field curve. For the original sample

$$H_c^{dec} = 0.863\ H_c^{inc},$$

and for the reduced sample

$$H_c^{dec} = 0.965\ H_c^{inc}.$$

This means that the magnetization was considerably more reversible for the reduced sample than for the original sample.

The Generalized Ginzburg-Landau Parameters

The first generalized Ginzburg-Landau parameter, $\kappa_1(t)$, was defined by Maki (47) to be

$$\kappa_1(t) = H_{c2}(t) \; / \sqrt{2}\, H_c(t) \; .$$

The values of $\kappa_1(t)/\kappa_1(1)$ are shown as a function of t in Figure 25 and are in good agreement with Sekula and Kernohan's values which are also shown in that figure. The second generalized Ginzburg-Landau parameter, $\kappa_2(t)$, was also introduced by Maki (47) and is defined by

$$\left(\frac{\partial(4\pi M)}{\partial H}\right)_{H_{c2}} = \frac{1}{1.159\,[2\,\kappa_2(t)^2 - 1]} \; .$$

The values of $\kappa_2(t)/\kappa_1(1)$ are also shown in Figure 25 and again are in good agreement with Sekula and Kernohan.

$\kappa_1(t)$ and $\kappa_2(t)$ are expected to approach the same limiting value, called simply κ, at t = 1. For this sample

$$\kappa_1(1) = \kappa_2(1) = \kappa = 0.82 \pm 0.02 \; ,$$

which is 3.5% lower than Sekula and Kernohan's value of 0.85 ± 0.02. Another parameter, κ_o, is defined as the intrinsic portion of κ and depends on the electronic structure of the material but is independent of the electronic mean free path. Goodman (48) has shown that κ_o can be found to a good approximation from

$$\kappa = \kappa_o + 7.53 \times 10^3 \sqrt{\gamma}\; \rho_o \; , \qquad (5)$$

where ρ_o is the normal state residual resistivity in Ω-cm and γ is the coefficient of the electronic portion of the normal state specific heat in erg cm^{-3} K^{-2}. We used Radebaugh and Keesom's value of

$$\gamma = 1.179 \times 10^{4} \text{ erg cm}^{-3} \text{ K}^{-2} .$$

The normal state residual resistivity, ρ_o, can be calculated from White and Woods' (49) value of

$$\rho_{295} - \rho_o = 1.99 \times 10^{-7} \ \Omega\text{-cm} ,$$

and the resistivity ratio of this sample, which is $\rho_{295}/\rho_o = 1500$. Solving these equations for ρ_o gives

$$\rho_o = 1.33 \times 10^{-8} \ \Omega\text{-cm} .$$

We now solve equation (5) to get $\kappa_o = 0.81 \pm 0.02$, which is in excellent agreement with Sekula and Kernohan's value of 0.82 ± 0.02.

Characteristic Lengths

The London penetration depth at $t = 0$, $\lambda_L(0)$, is related to κ and $\left|dH_c/dt\right|_{t=1}$ in the following way (37)

$$\lambda_L(0) = \left[\frac{\pi\sqrt{2}}{\varphi_o \kappa}\left|\frac{dH_c}{dt}\right|_{t=1}\right]^{-\frac{1}{2}} .$$

For this sample $\left|dH_c/dt\right|_{t=1} = 2.78 \times 10^{3}$ Oe, hence $\lambda_L(0) = 371$ Å, which compares very favorably with Sekula and Kernohan's value of 375 Å. The coherence distance, ξ_o, is related to κ_o and $\lambda_L(0)$ and can be calculated (2) from the expression

$$\kappa_o = 0.96 \ \lambda_L(0) \ / \ \xi_o .$$

For this sample one finds $\xi_o = 440$ Å which agrees exactly with Sekula and Kernohan's value.

An average value of the electronic mean free path, ℓ, can be calculated (40) from the free electron gas expression

$$\rho_o \ell = \pi^2 k_B^2 / (e^2 \gamma V_F)$$

where ρ_o is the normal state residual resistivity, k_B is the Boltzmann constant, e is the electronic charge, γ is the coefficient of the electronic portion of the normal state specific, and V_F is the average Fermi velocity. Values of γ and ρ_o were reported in the previous section. The average Fermi velocity, V_F, can be calculated (5) from the expression

$$\xi_o = 0.18 \hbar V_F / (k_B T_c).$$

Hence

$$\ell = \frac{\pi^2 k_B (0.18) \hbar}{\rho_o e^2 \gamma \xi_o T_c} = 2.69 \times 10^{-4} \text{ cm.}$$

This means ℓ/ξ_o is 61 for our vanadium, whereas Sekula and Kernohan's sample had ℓ/ξ_o approximately equal to 20.

DISCUSSION

The purpose of this work was to look for a first-order phase transition at H_{c1} in very pure vanadium which is a long mean free path, low-κ type-II material. A first-order transition would indicate that there was an attractive interaction between fluxoids so that an intermediate mixed state would exist in the sample for an applied field greater than $H_{c1}(1-D)$ and less than $H_{c1}(1-D) + D\,B_o$. The magnetization data reported in this work do not establish conclusively whether the transition at H_{c1} is first-order, and hence whether or not the intermediate mixed state exists in vanadium. The results were inconclusive because, although the magnetization curves dropped quite steeply near H_{c1}, they did not drop so steeply as predicted by the demagnetizing factor associated with the sample geometry. The data were analyzed under the assumption that the transition was first-order to obtain B_o and d_o because considerable evidence exists that the intermediate mixed state does occur in other low-κ type-II materials. Before discussing that evidence, it must be pointed out that decoration experiments on vanadium (30, 44) have so far failed to show any evidence of the existence of the intermediate mixed state. However, the results reported so far are not sufficient to rule out the possibility that such a state does occur.

Evidence which favors the occurence of the intermediate mixed state in vanadium is found in the magnetic behavior of other low-κ type-II materials. There is excellent evidence that the intermediate mixed state occurs in niobium. This has been established by the decoration experiments of Krägeloh (12, 13) and Essmann and Träuble (14, 26-30), which

clearly show the coexistence of a flux-line lattice adjacent to pure Meissner regions in the sample. In addition, magnetization data for niobium showing the characteristic kink just above H_{c1} have been published by Finnemore, Clem, and Stromberg (36). Those magnetization curves, although they did show a kink, also failed to drop at the slope predicted by the geometrical demagnetizing factor. Because niobium and vanadium are the only two pure elements which show type-II behavior, we expect their properties to be very similar.

Further evidence for the existence of the intermediate mixed state is found in the magnetization data taken by Auer and Ullmaier (37) on tantalum-nitrogen alloys which have κ near the value $1/\sqrt{2}$. The present work is similar to Auer and Ullmaier's in that the samples have similar values of κ, but differs in that our vanadium has an electronic mean free path which is sixty to seventy times longer than that of any of the TaN samples used by Auer and Ullmaier.

Auer and Ullmaier's magnetization data show that samples with κ between 0.5 and 1.1 undergo a first-order transition at H_{c1} at some temperatures. Samples with κ slightly less than $1/\sqrt{2}$ show type-II behavior with a first-order transition at H_{c1} at low temperatures, but show type-I behavior near T_c. The explanation for this is that $\kappa_1(t)$ decreases as t increases. Auer and Ullmaier have found that a sample displays type-I behavior for $\kappa_1(t) < 1/\sqrt{2}$ and hence type-I and type-II behavior can be observed in the same sample at various temperatures. Similarly, they have found that samples with κ slightly greater than $1/\sqrt{2}$ can show a type-II behavior with a first-order transition near H_{c1} at low temperatures, but

near T_c the transition at H_{c1} becomes second-order. The explanation for this behavior is much more complex and speculative. By measuring a number of samples with different values of κ, Auer and Ullmaier constructed the phase diagram shown in Figure 26, which shows what type of magnetic behavior is expected for TaN alloys with κ near $1/\sqrt{2}$ at various values of the reduced temperature, t.

The theory of Leung and Jacobs (25) predicts a phase diagram for a relatively short mean free path material which agrees qualitatively with that found by Auer and Ullmaier. In addition, Leung and Jacobs have predicted a phase diagram which would apply to pure metals like vanadium. That diagram, shown in Figure 27, predicts that a sample with $\kappa = 0.82$ will show a first-order transition at H_{c1} for $t \leq 0.85$ but may possibly show a second-order transition for $t \geq 0.85$. Unfortunately our data are not sensitive enough to detect whether there is indeed some critical value of $t \geq 0.85$ for which the transition becomes second-order in vanadium. The rounding near the transition and the degree of arbitrariness in our definition of the kink preclude any definite determination of whether the kink actually disappears at some temperature.

Finally, it is interesting to note that in this work B_o was observed to be approximately one-fourth of H_{c2} at all temperatures. The values of H_{c2}/B_o obtained for the runs on the original sample averaged 4.2 ± 0.5. For the reduced sample H_{c2}/B_o was 3.8. This may be merely a coincidence or may indicate some fundamental relationship between the flux density at initial flux penetration and the flux density when the material becomes normal at H_{c2}.

FIGURES

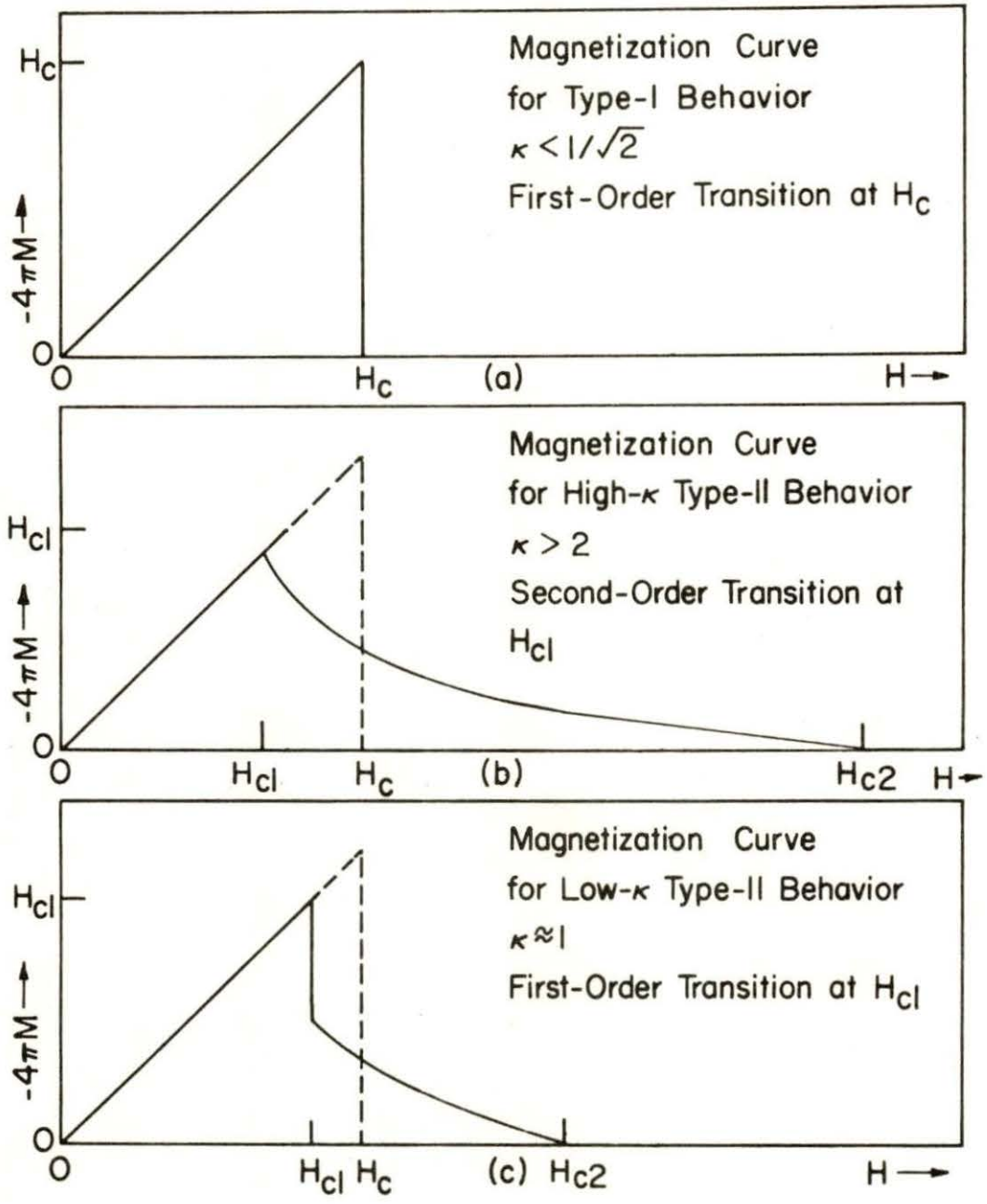

Figure 1. Ideal magnetization curves for (a) type-I, (b) high-κ type-II, and (c) low-κ type-II materials.

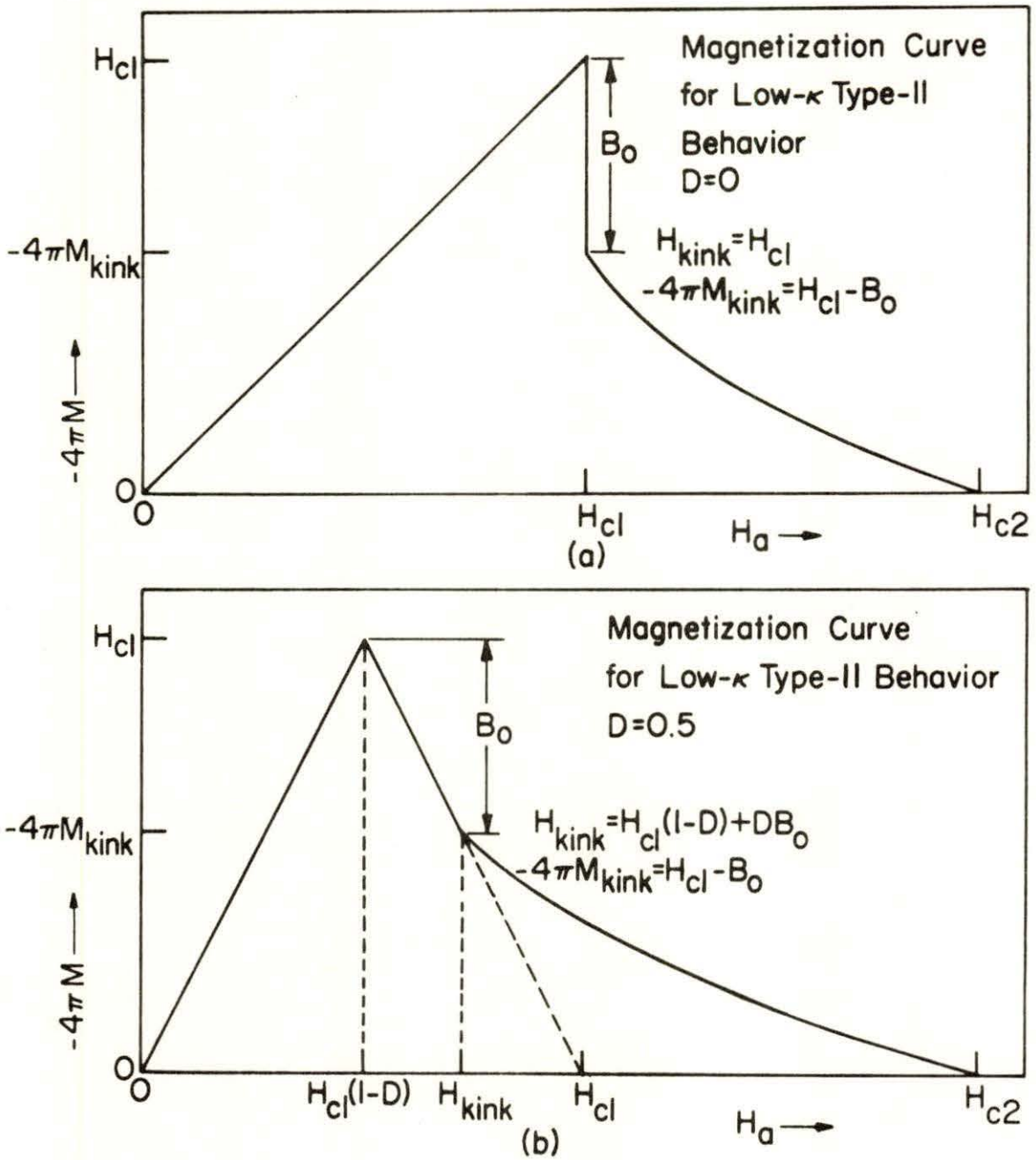

Figure 2. Ideal magnetization curves for low-κ type-II materials with (a) D = 0 and (b) D = 0.5, where D is the demagnetizing factor.

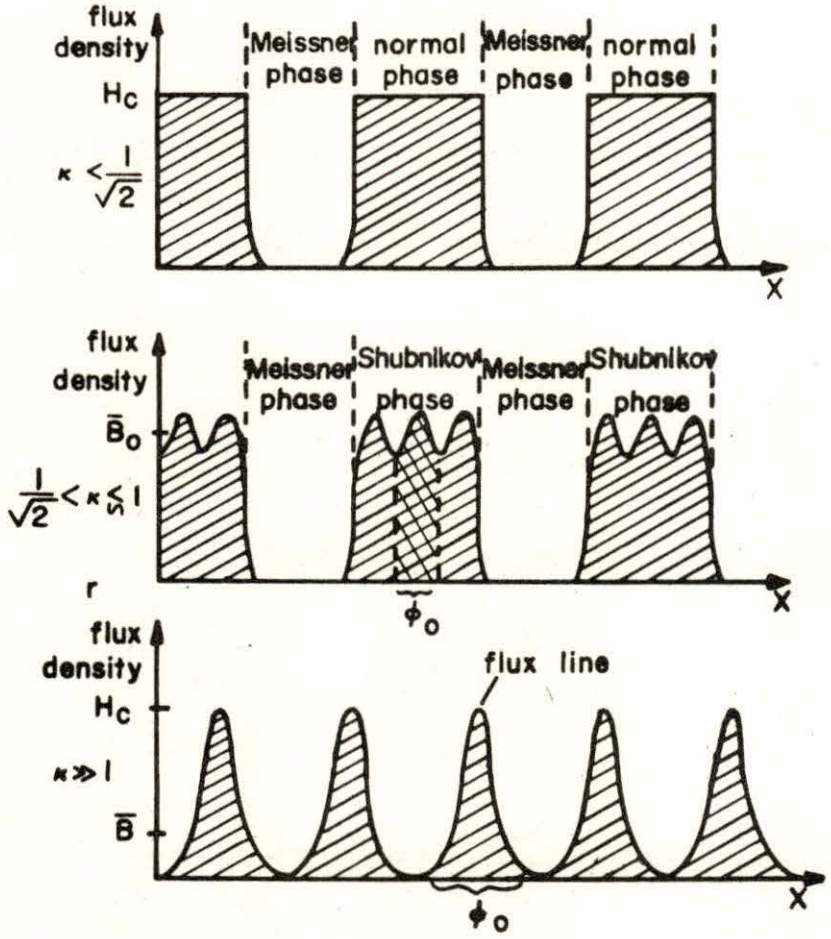

Figure 3. Flux density versus distance for (a) type-I behavior, (b) low-κ type-II behavior, and (c) high-κ type-II behavior. See Reference 38.

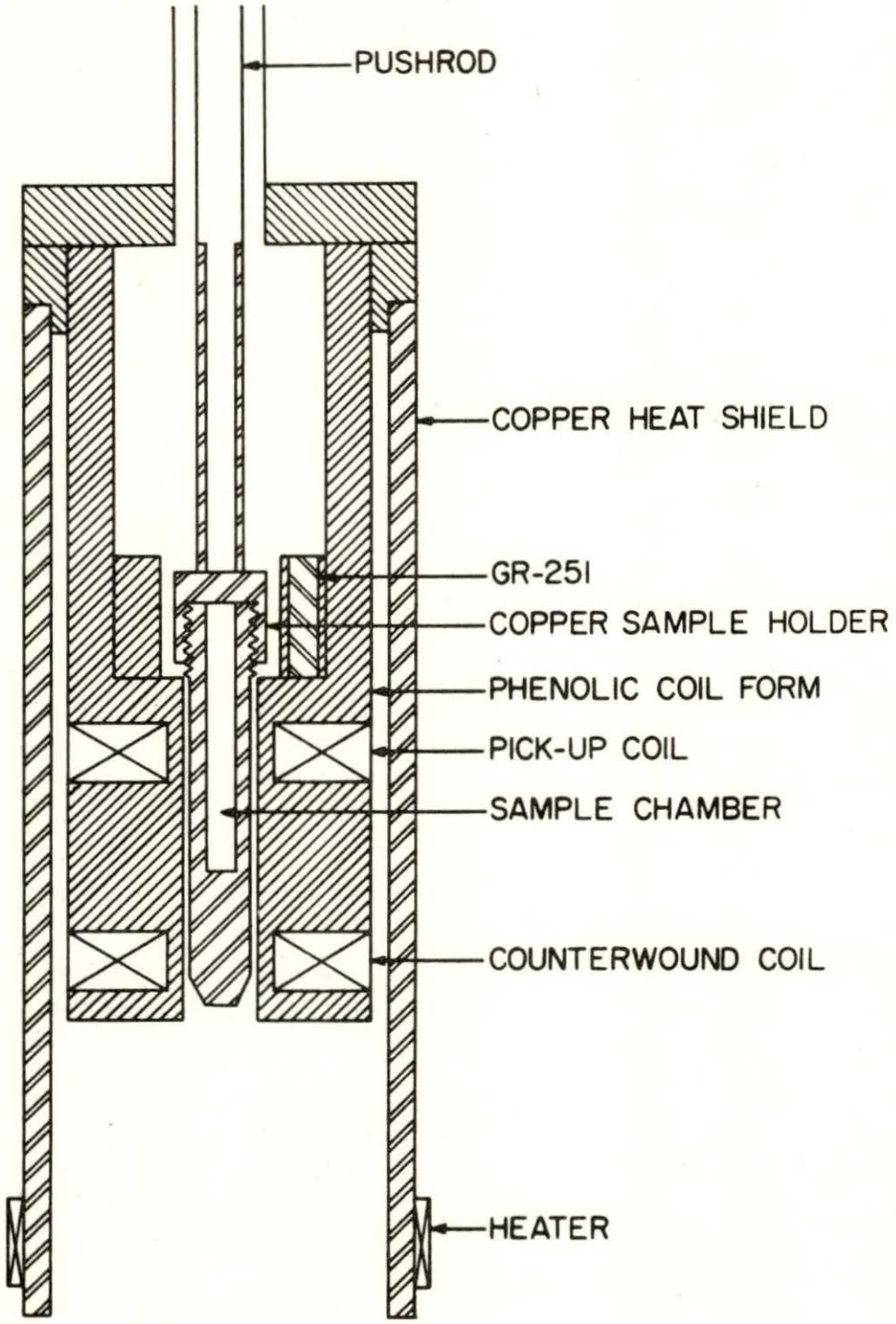

Figure 4. Cryostat.

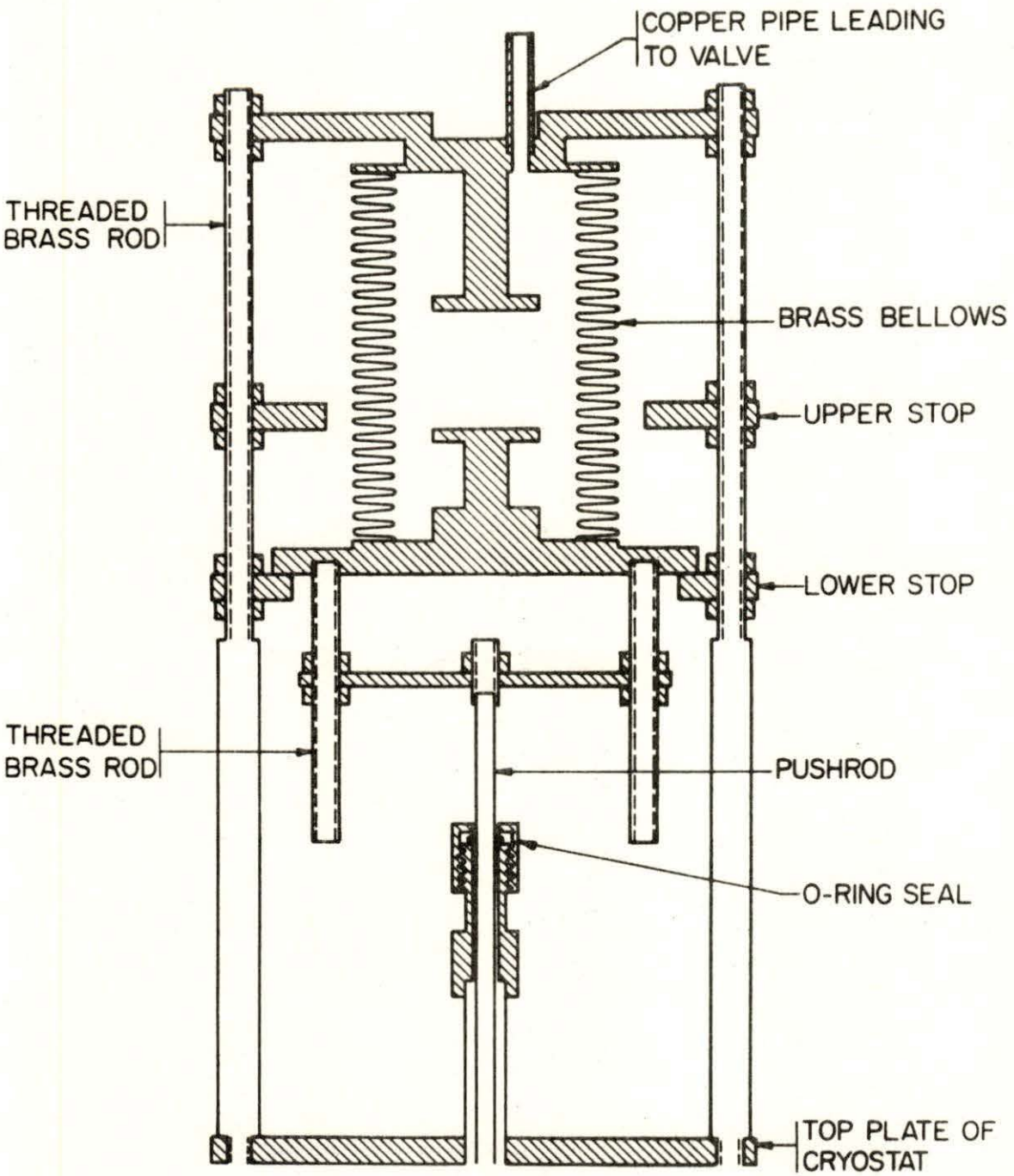

Figure 5. Sample-lifting device.

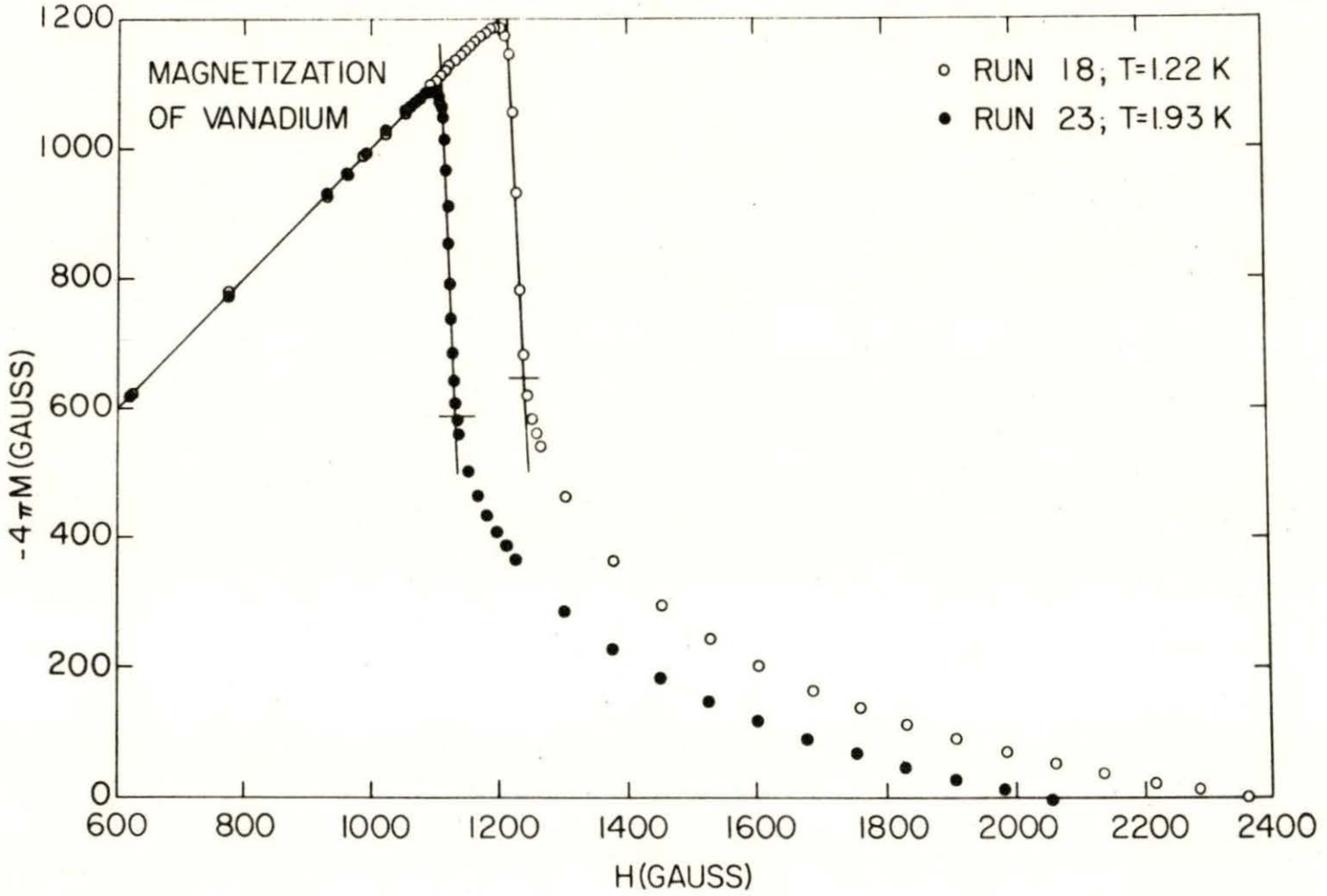

Figure 6. Magnetization of vanadium at T = 1.22 and 1.93 K.

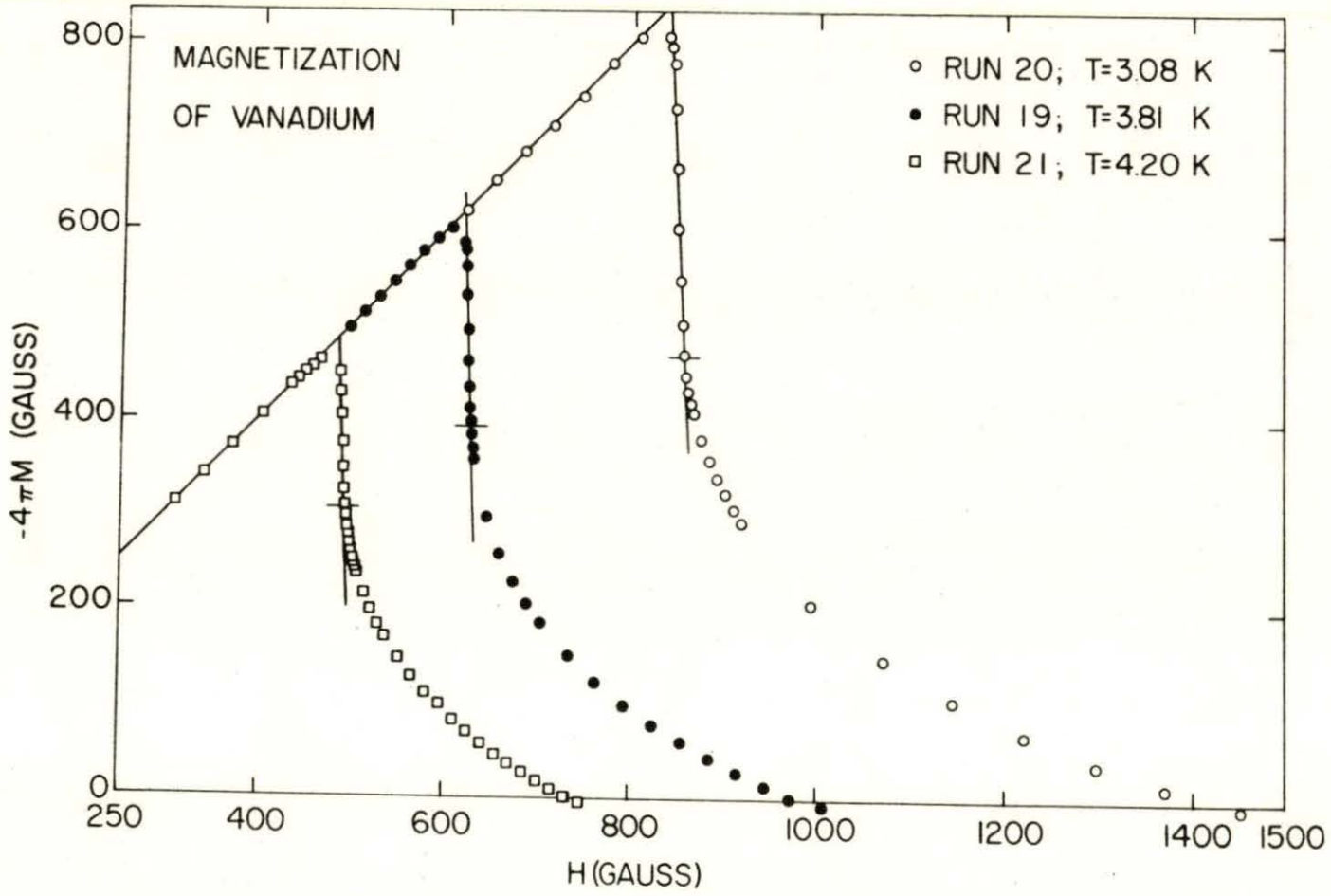

Figure 7. Magnetization of vanadium at T = 3.08, 3.81, and 4.20 K.

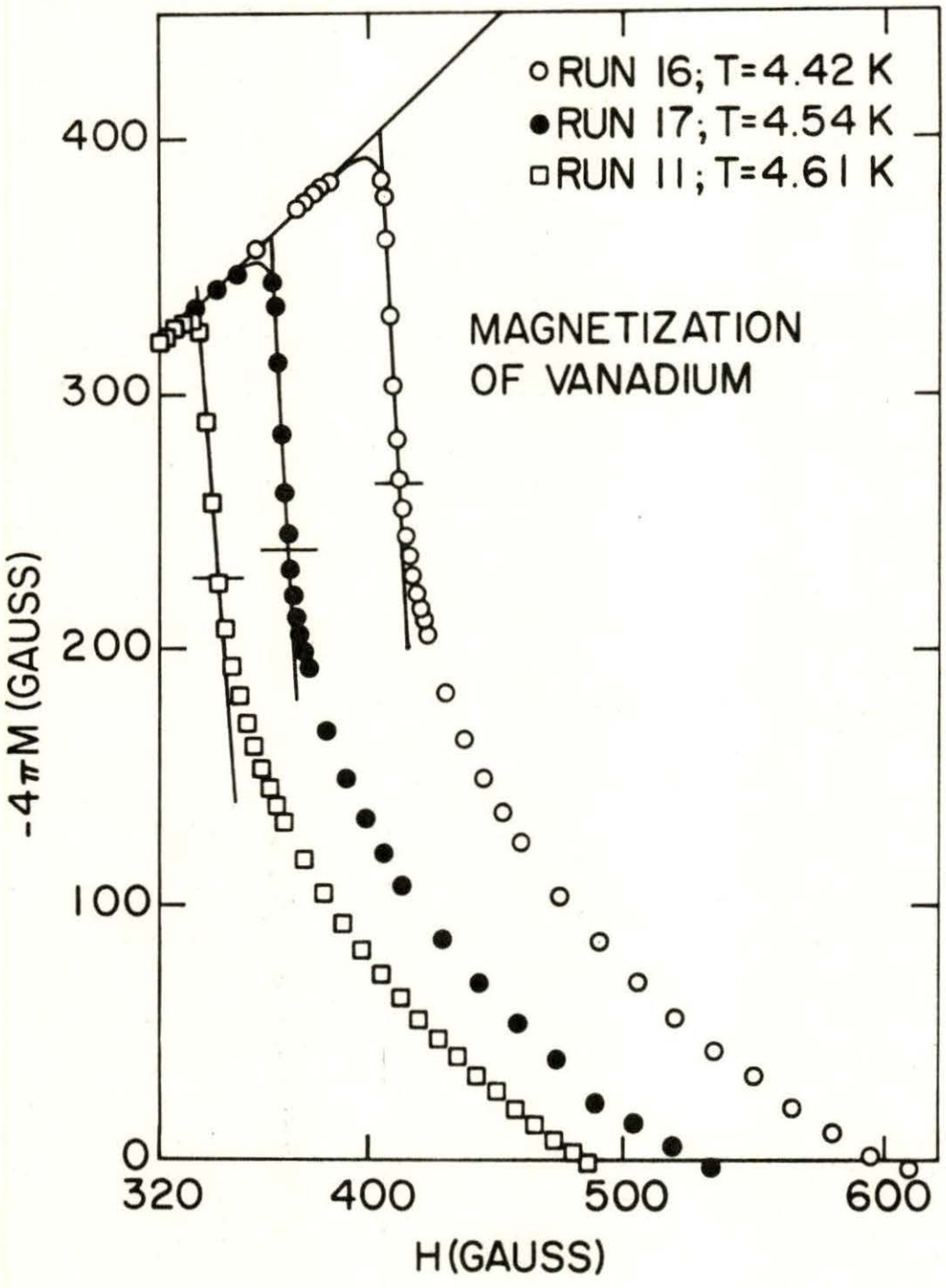

Figure 8. Magnetization of vanadium at T = 4.42, 4.54, and 4.61 K.

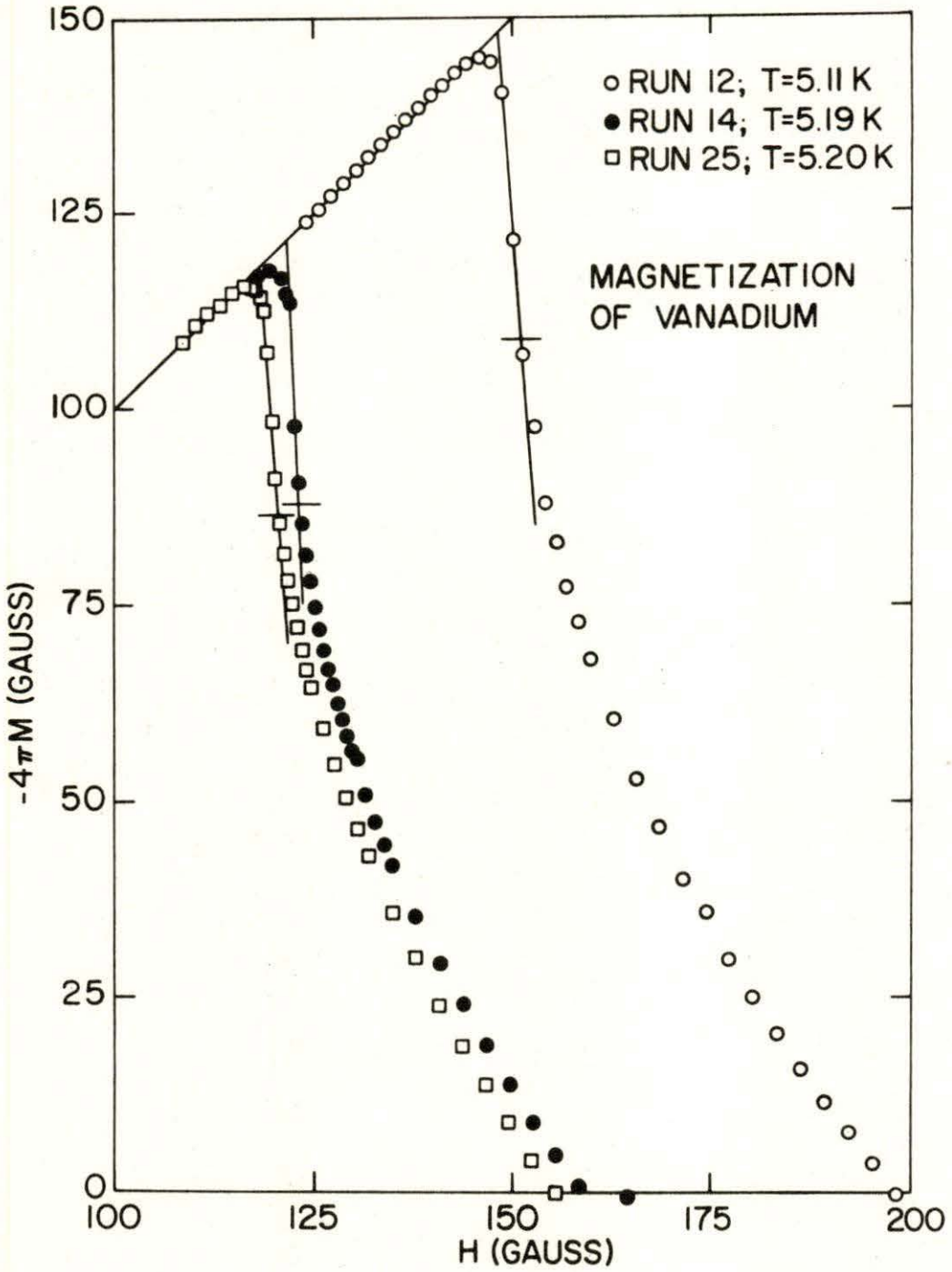

Figure 9. Magnetization of vanadium at T = 5.11, 5.19, and 5.20 K.

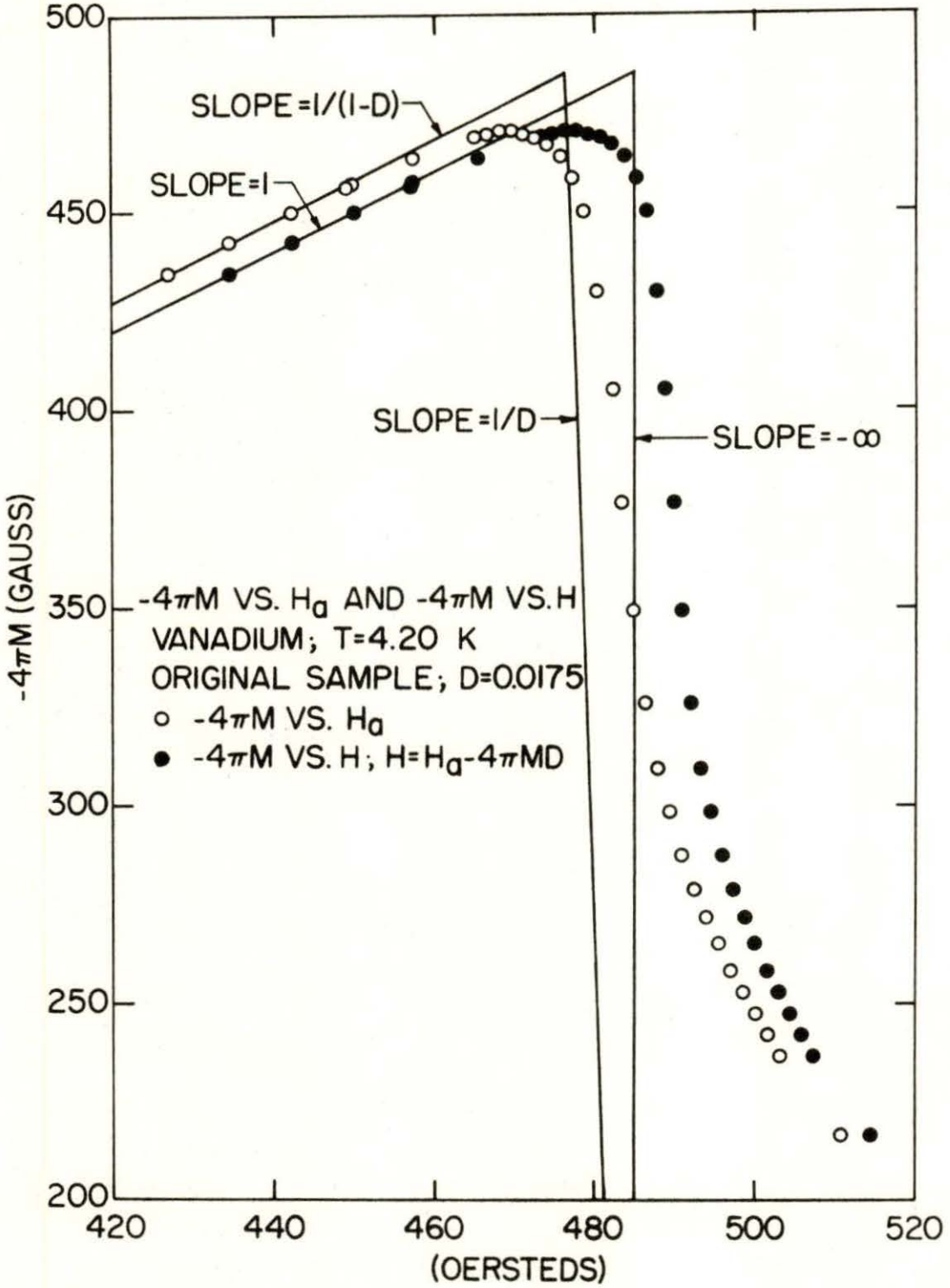

Figure 10. $-4\pi M$ versus H_a and $-4\pi M$ versus H at T = 4.20 K.

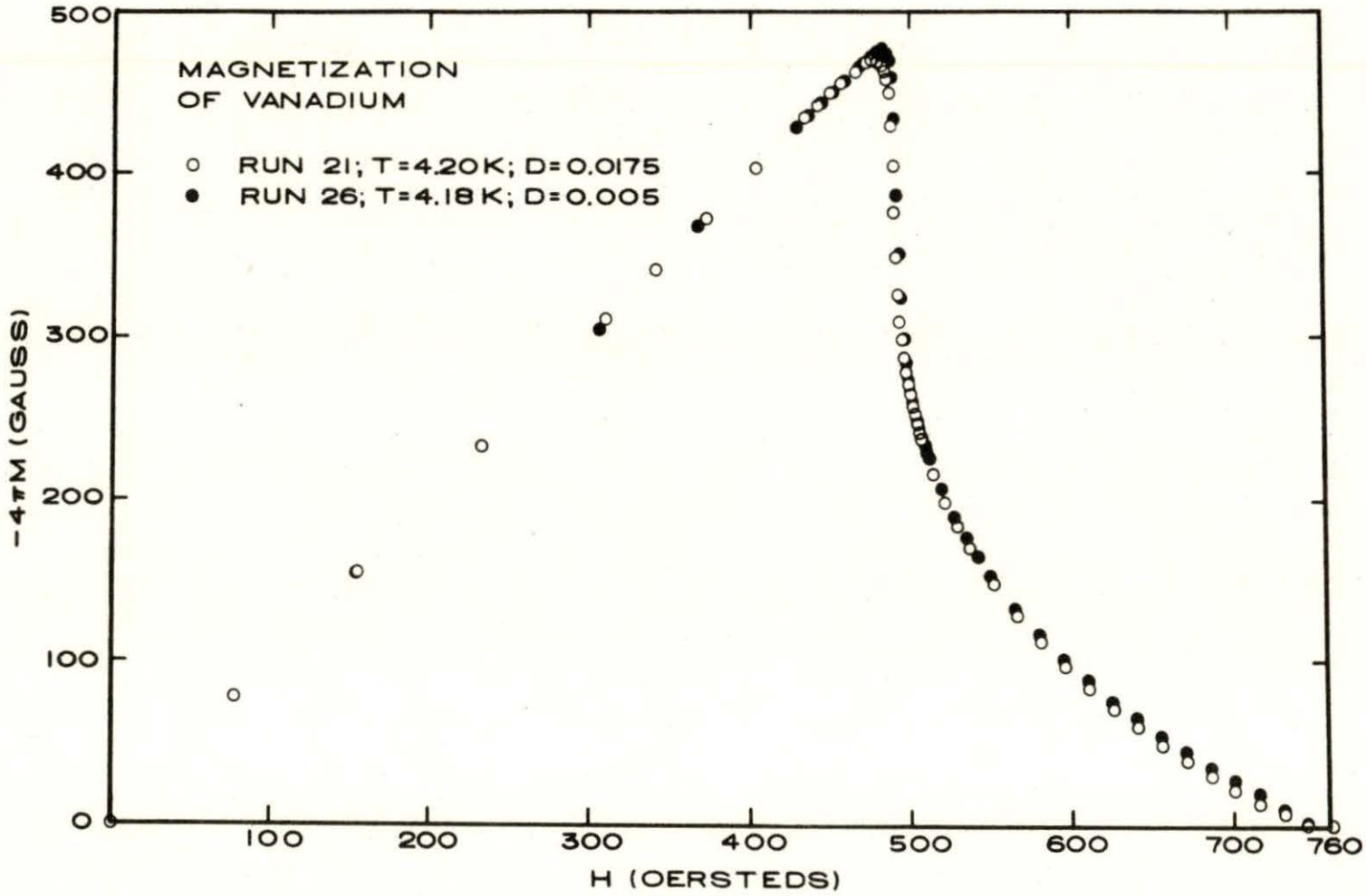

Figure 11. Comparison between magnetization curves for the original and reduced samples.

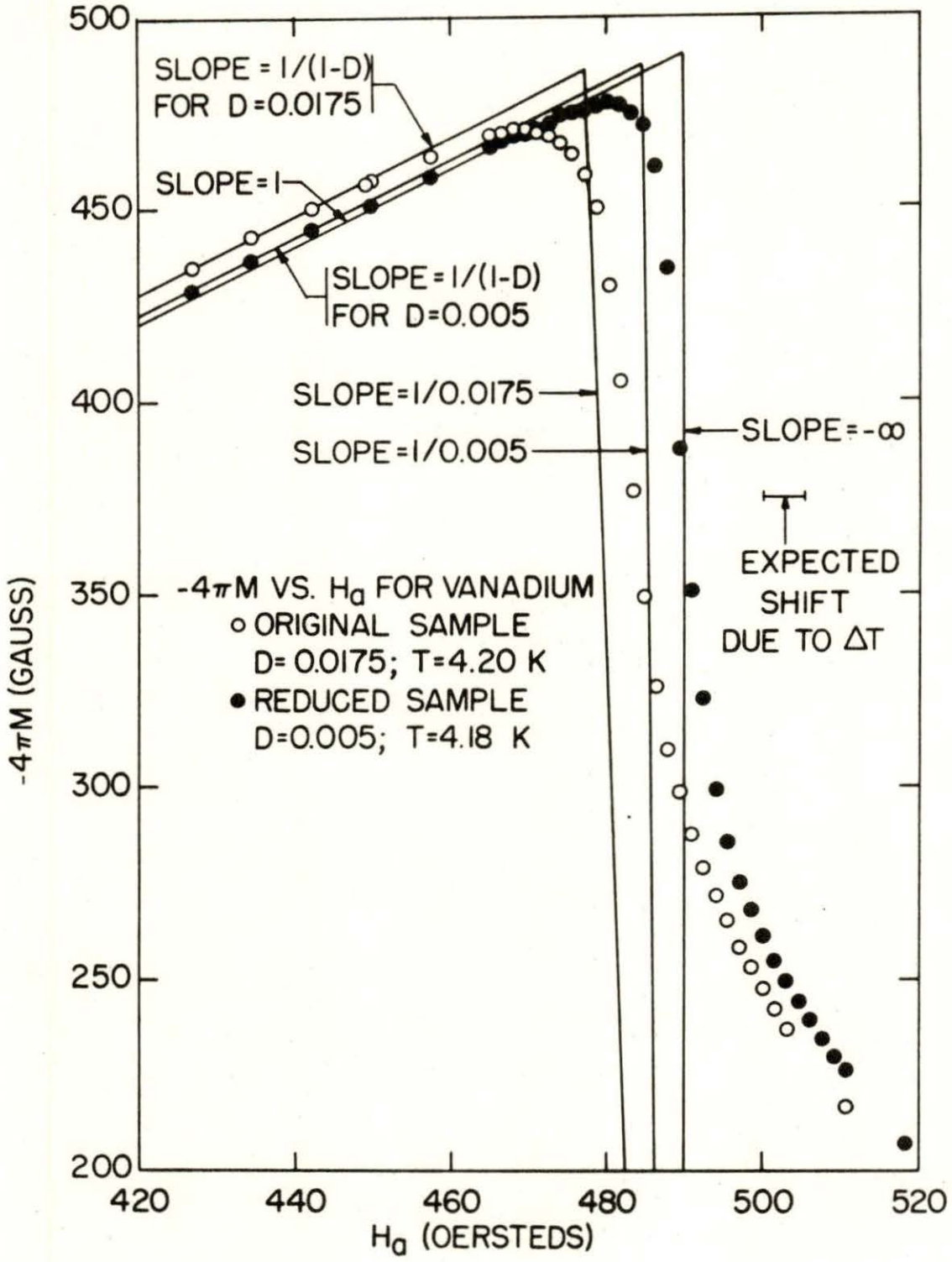

Figure 12. $-4\pi M$ versus H_a for original sample and reduced sample.

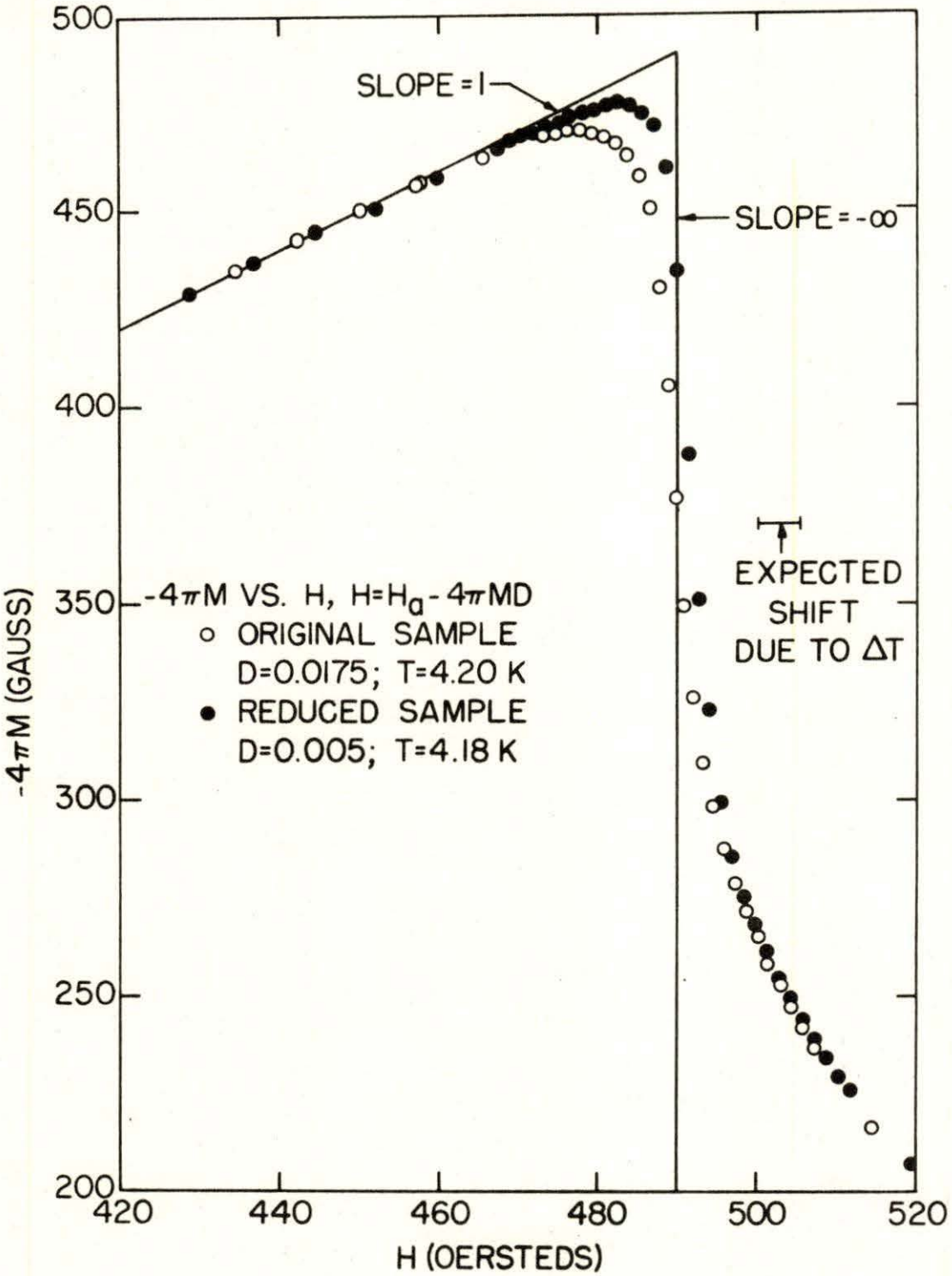

Figure 13. $-4\pi M$ versus H for original sample and reduced sample.

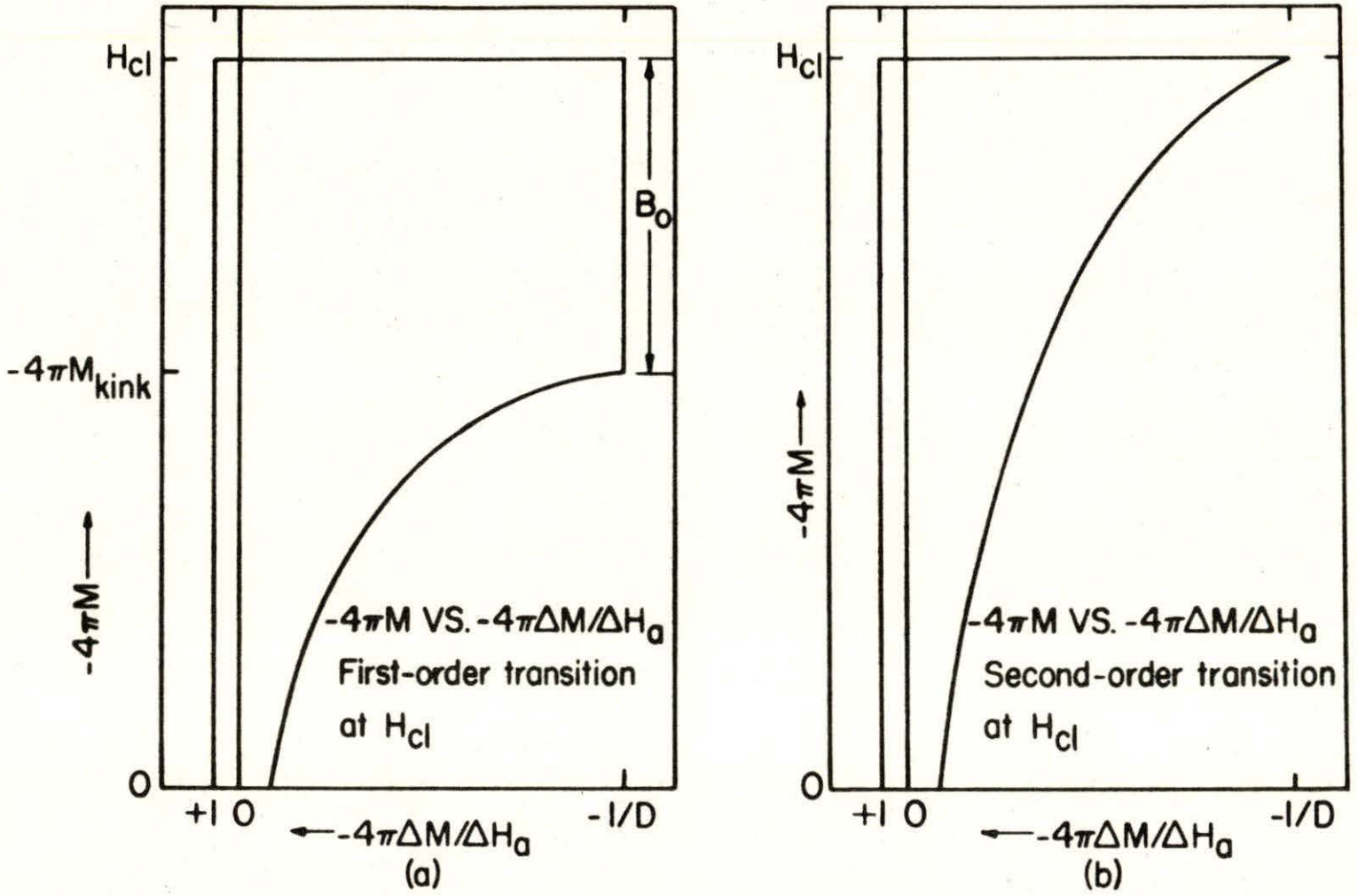

Figure 14. Ideal $-4\pi M$ versus $-4\pi\Delta M/\Delta H$ for (a) a first-order transition at H_{cl} and (b) a second-order transition at H_{cl}.

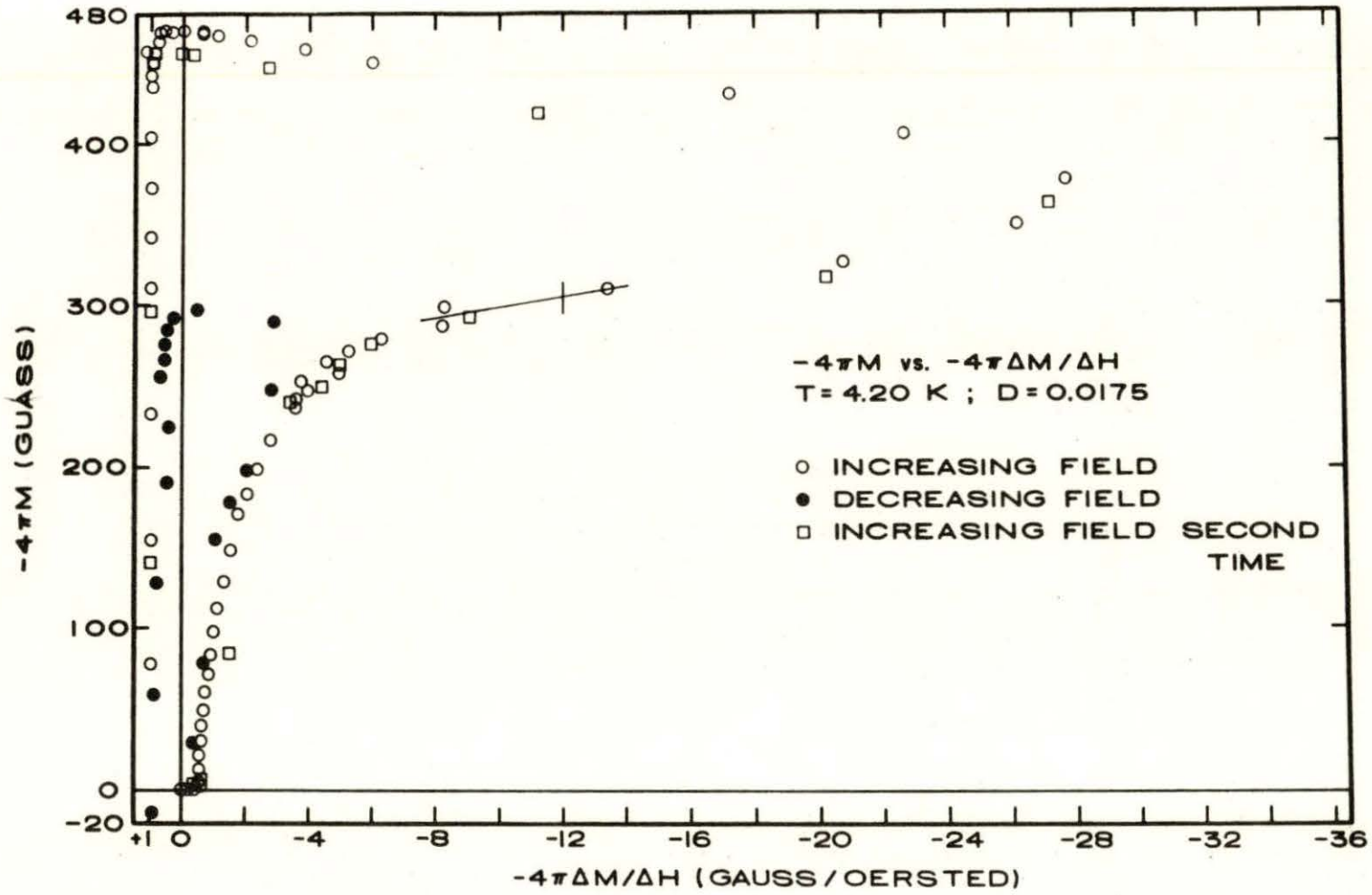

Figure 15. $-4\pi M$ versus $-4\pi\Delta M/\Delta H$ for the original sample.

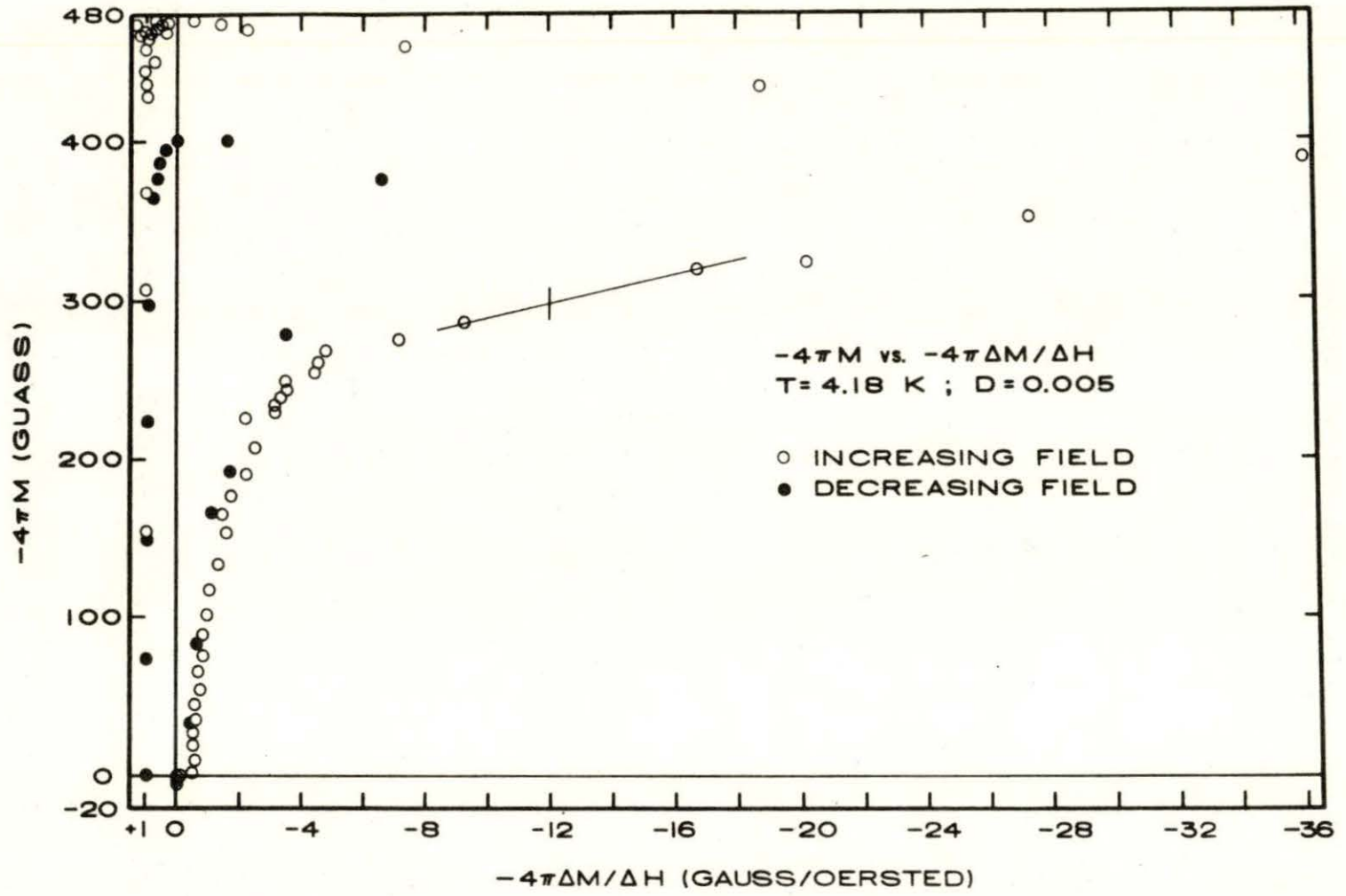

Figure 16. $-4\pi M$ versus $-4\pi\Delta M/\Delta H$ for the reduced sample.

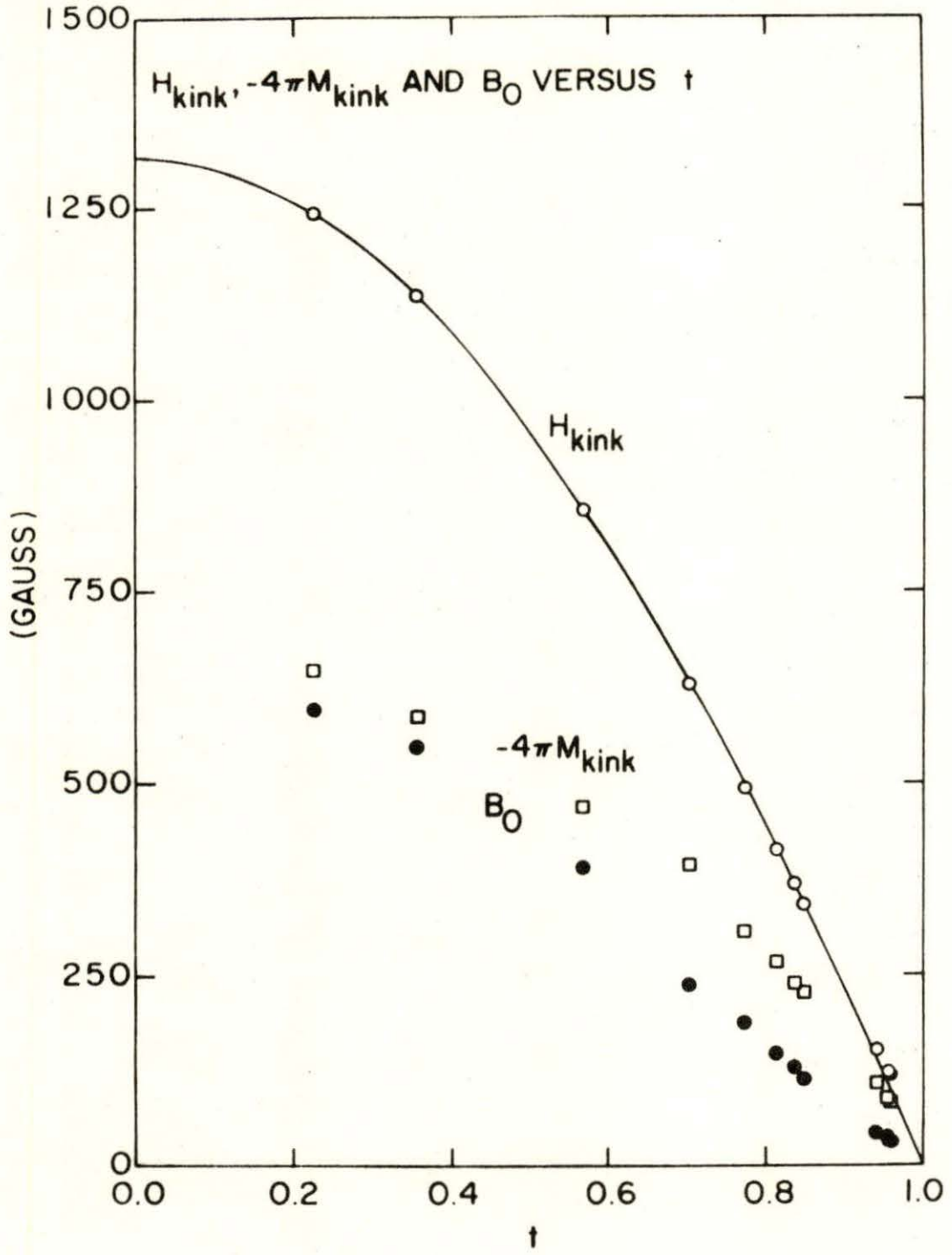

Figure 17. H_{kink}, $-4\pi M_{kink}$, and B_o versus $t = T/T_c$.

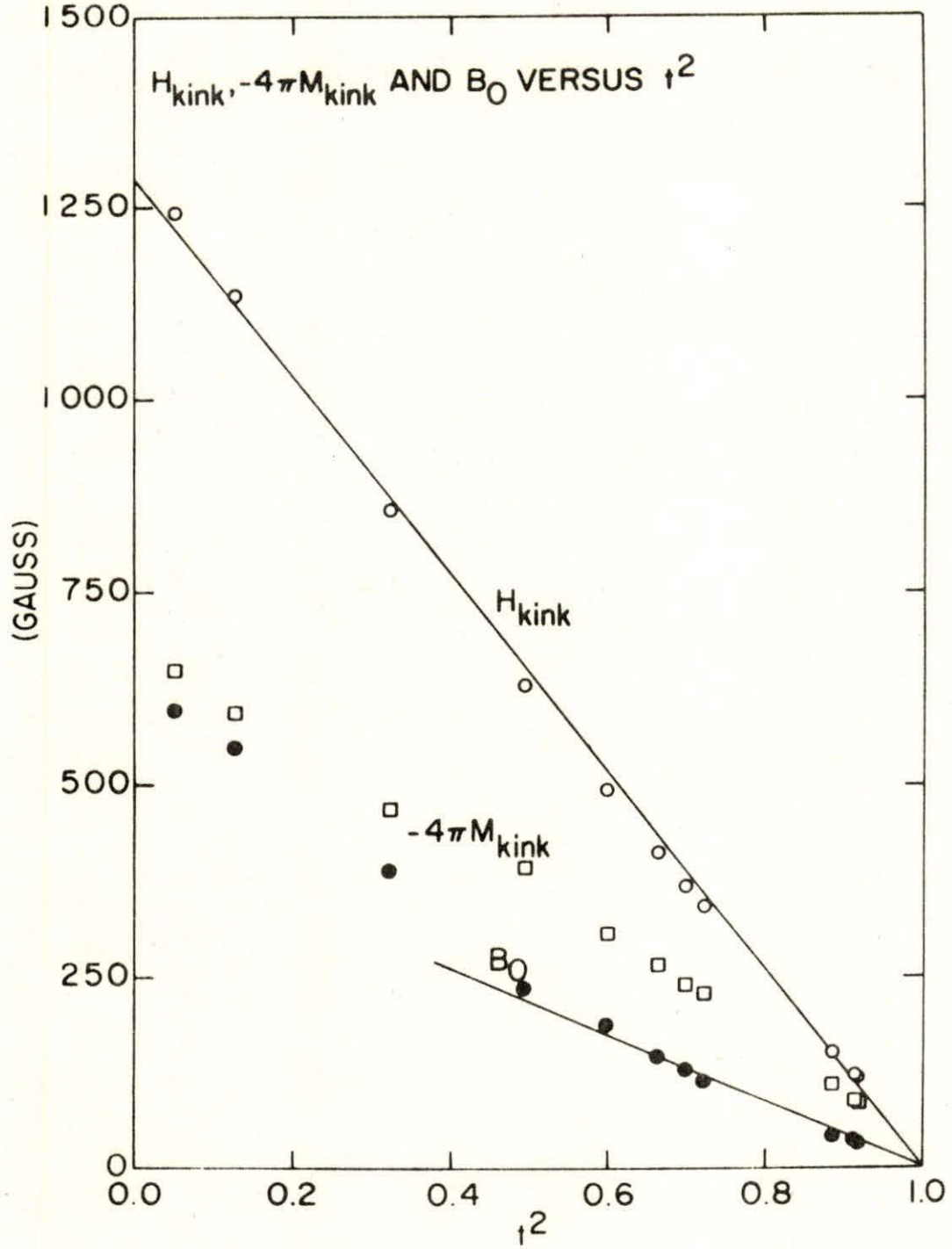

Figure 18. H_{kink}, $-4\pi M_{kink}$, and B_o versus t^2.

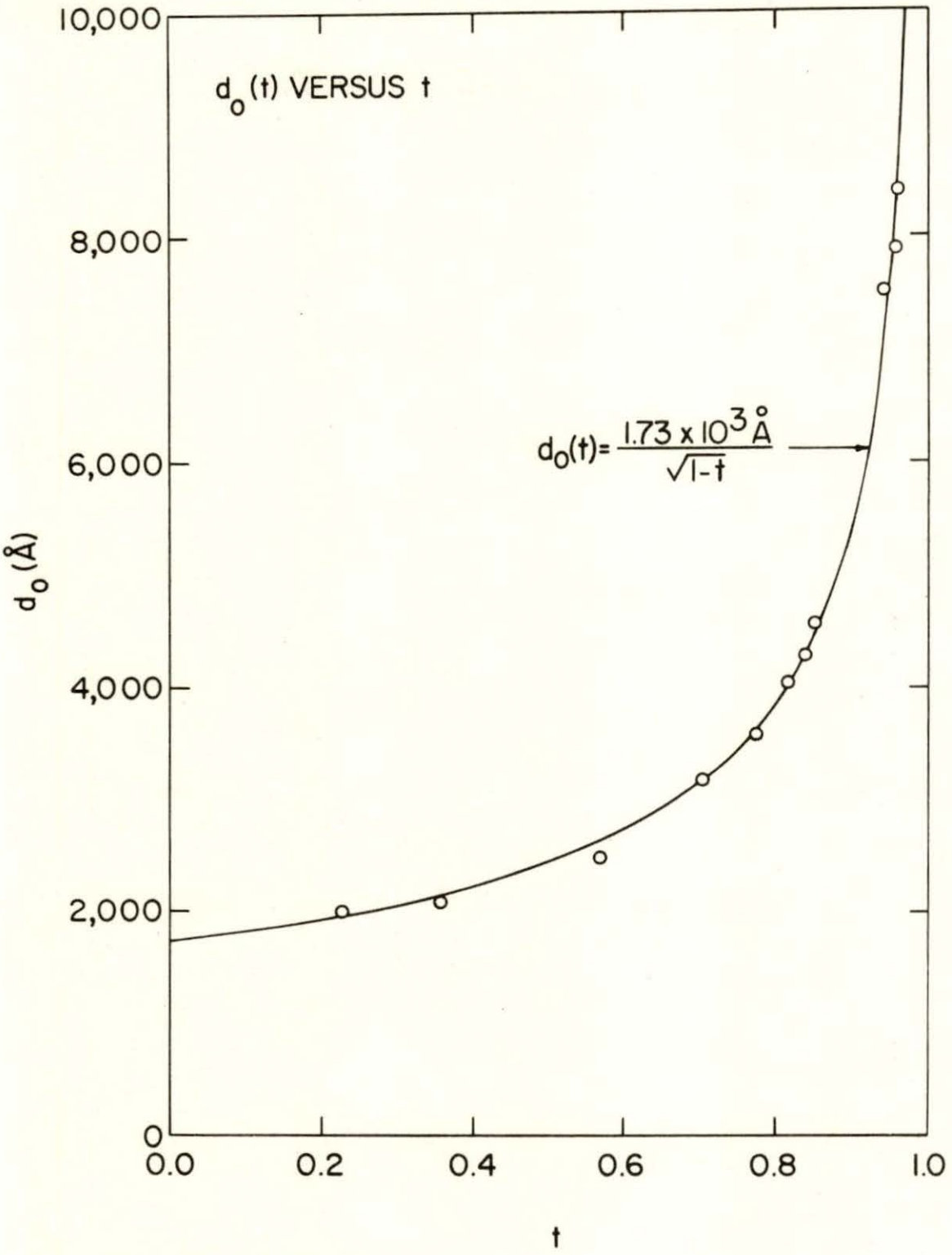

Figure 19. $d_o(t)$ versus t.

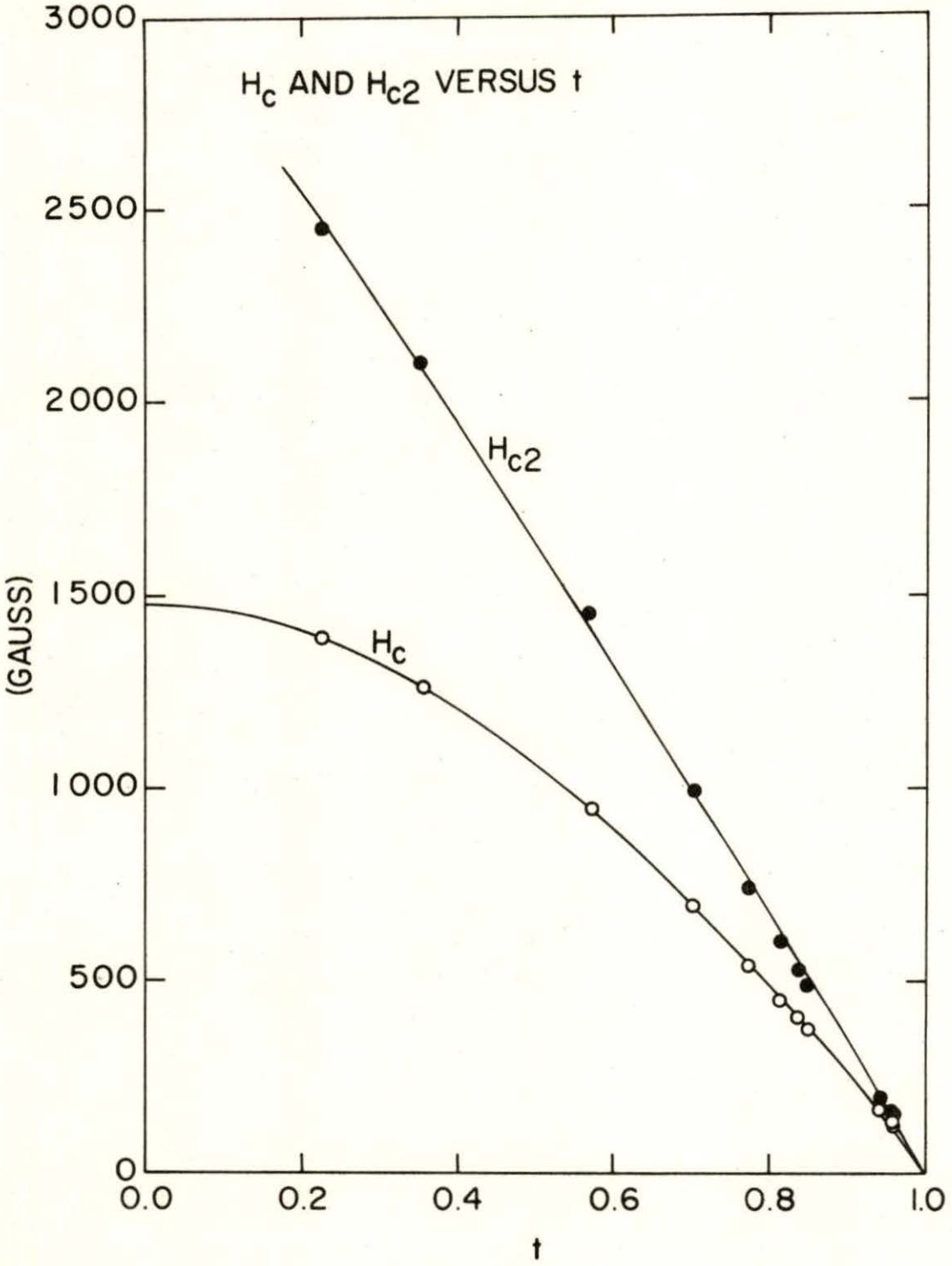

Figure 20. H_c and H_{c2} versus t.

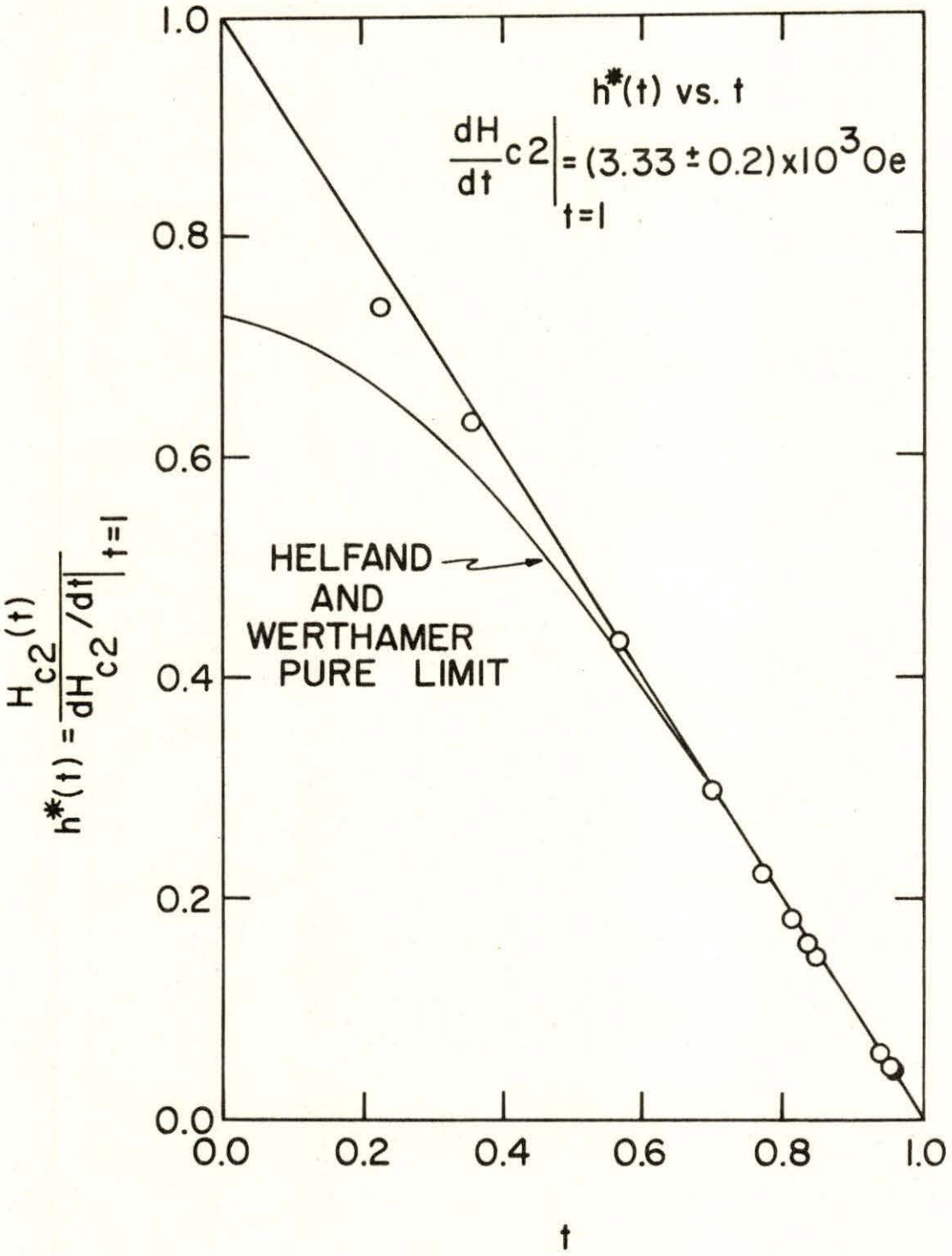

Figure 21. $h^{*}(t)$ versus t.

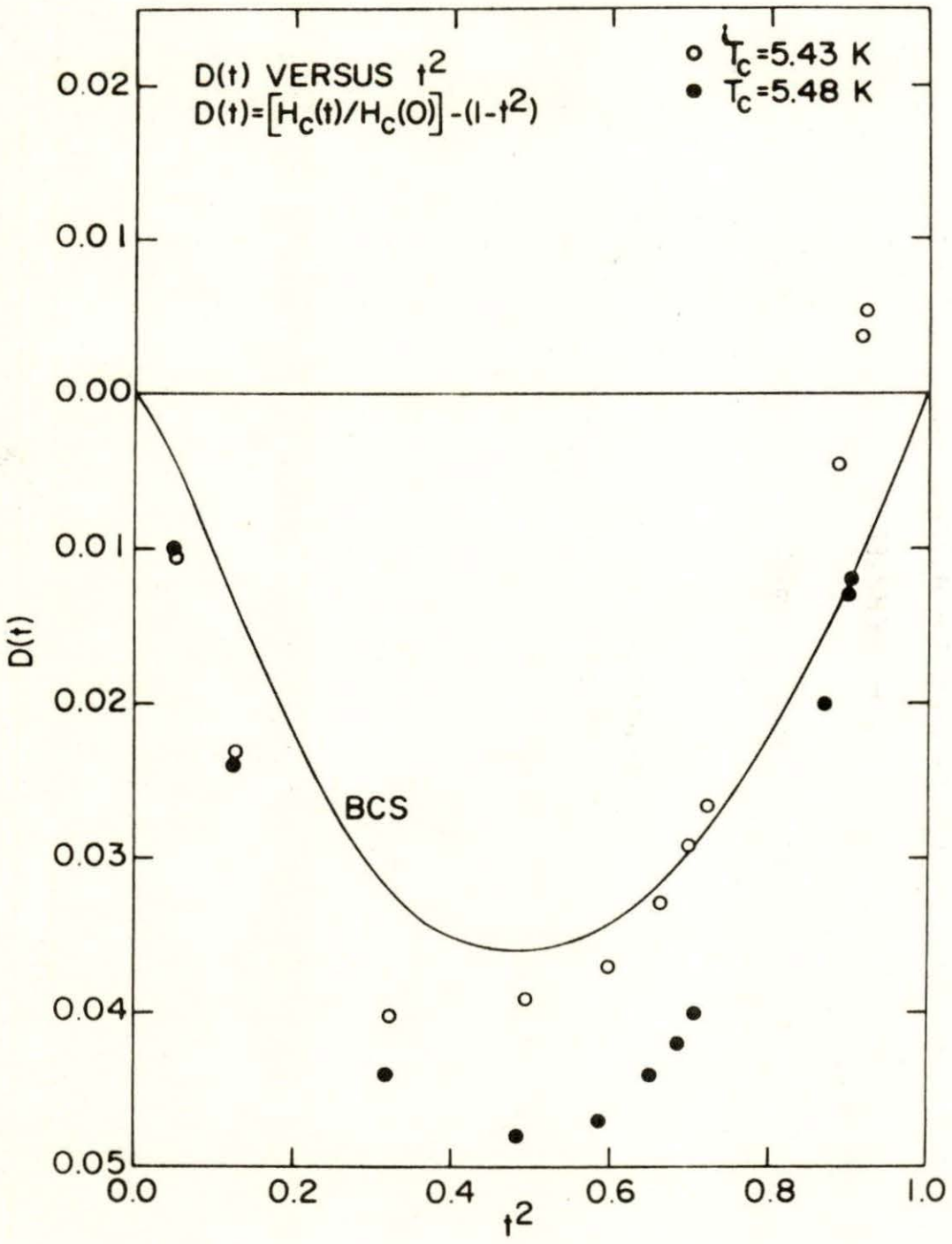

Figure 22. Deviation plot, D(t) versus t.

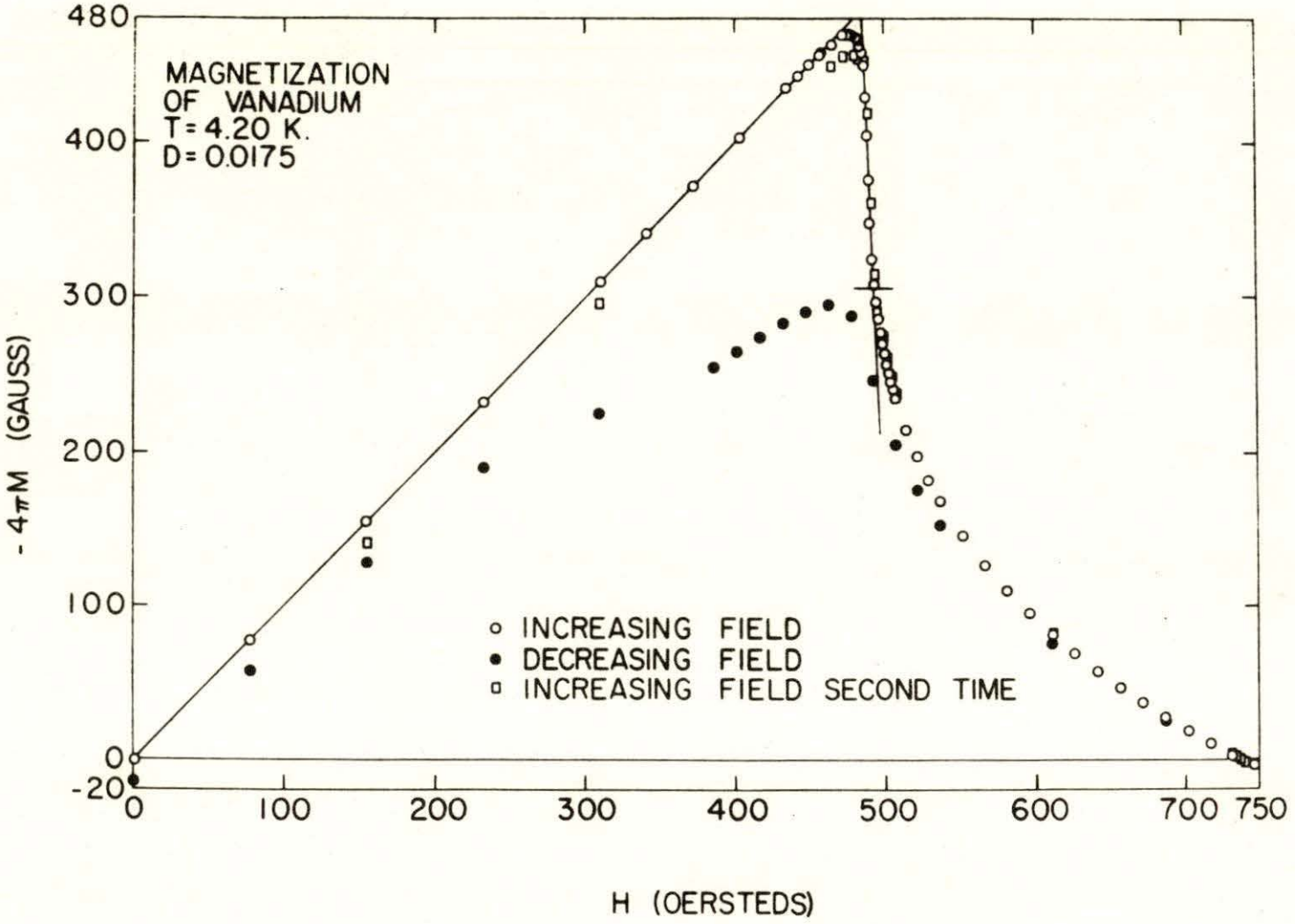

Figure 23. Complete magnetization curve for the original sample at T = 4.20 K.

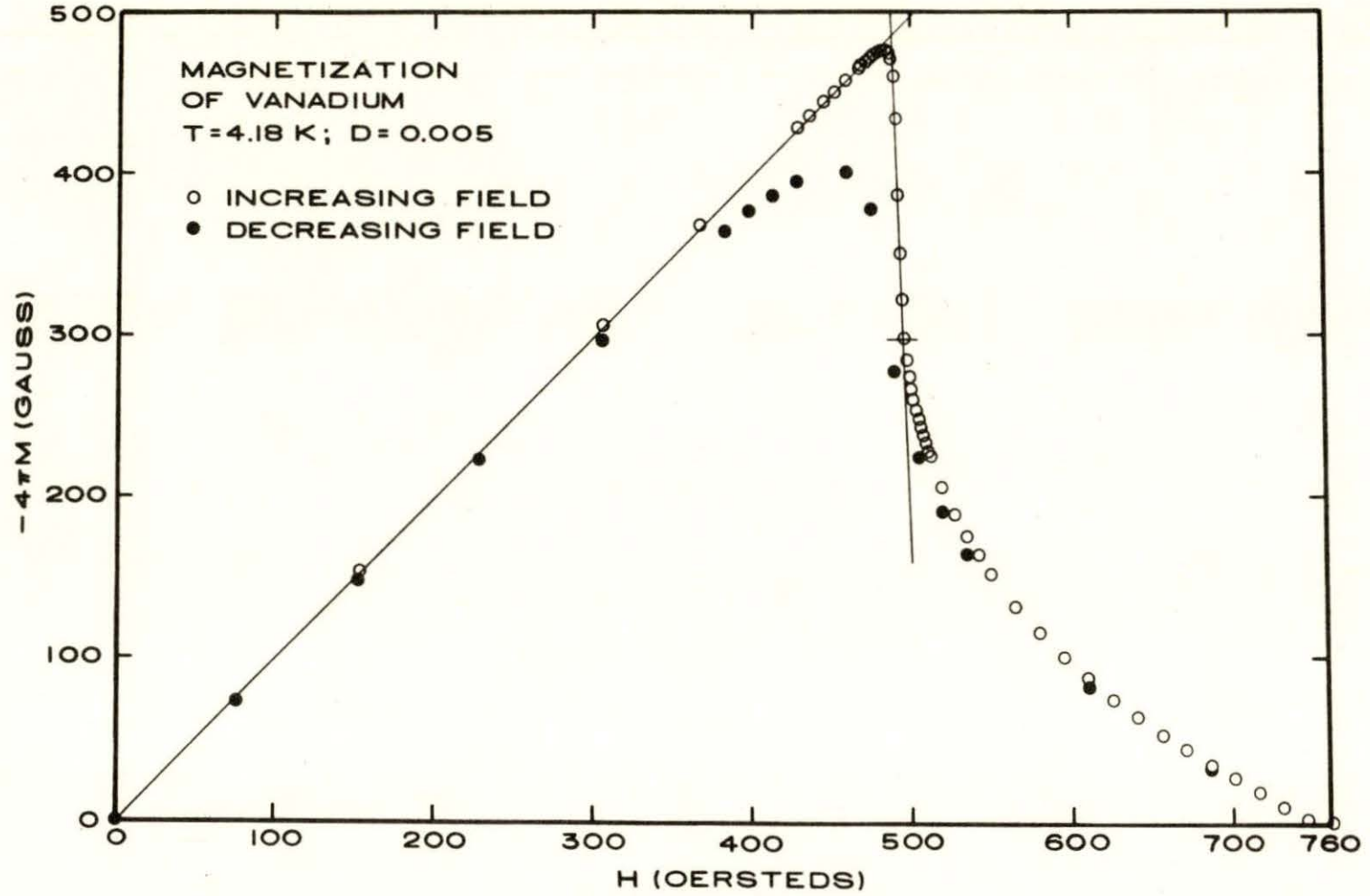

Figure 24. Complete magnetization curve for the reduced sample at T = 4.18 K.

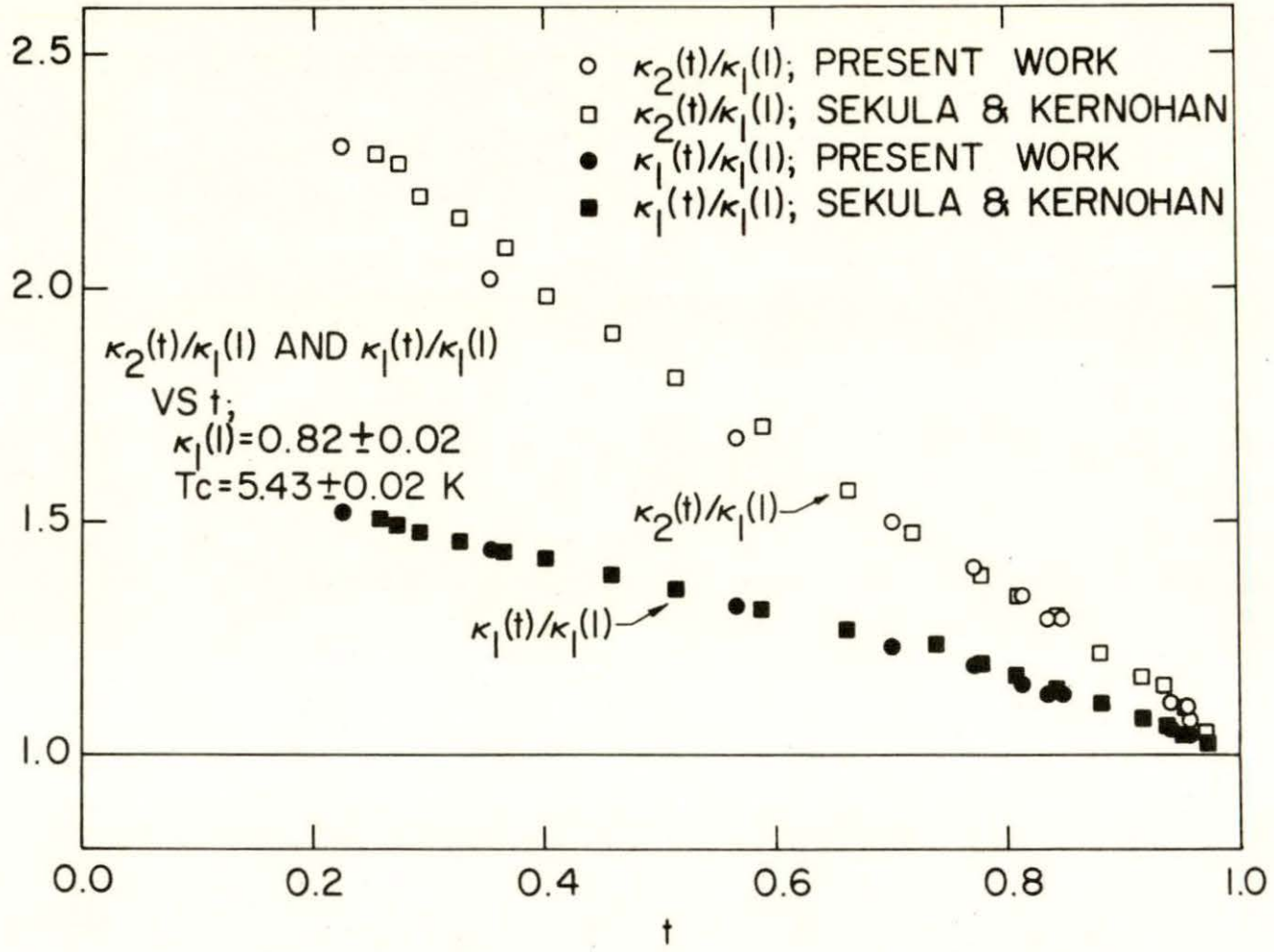

Figure 25. $\kappa_1(t)/\kappa_1(1)$ and $\kappa_2(t)/\kappa_1(1)$ versus t.

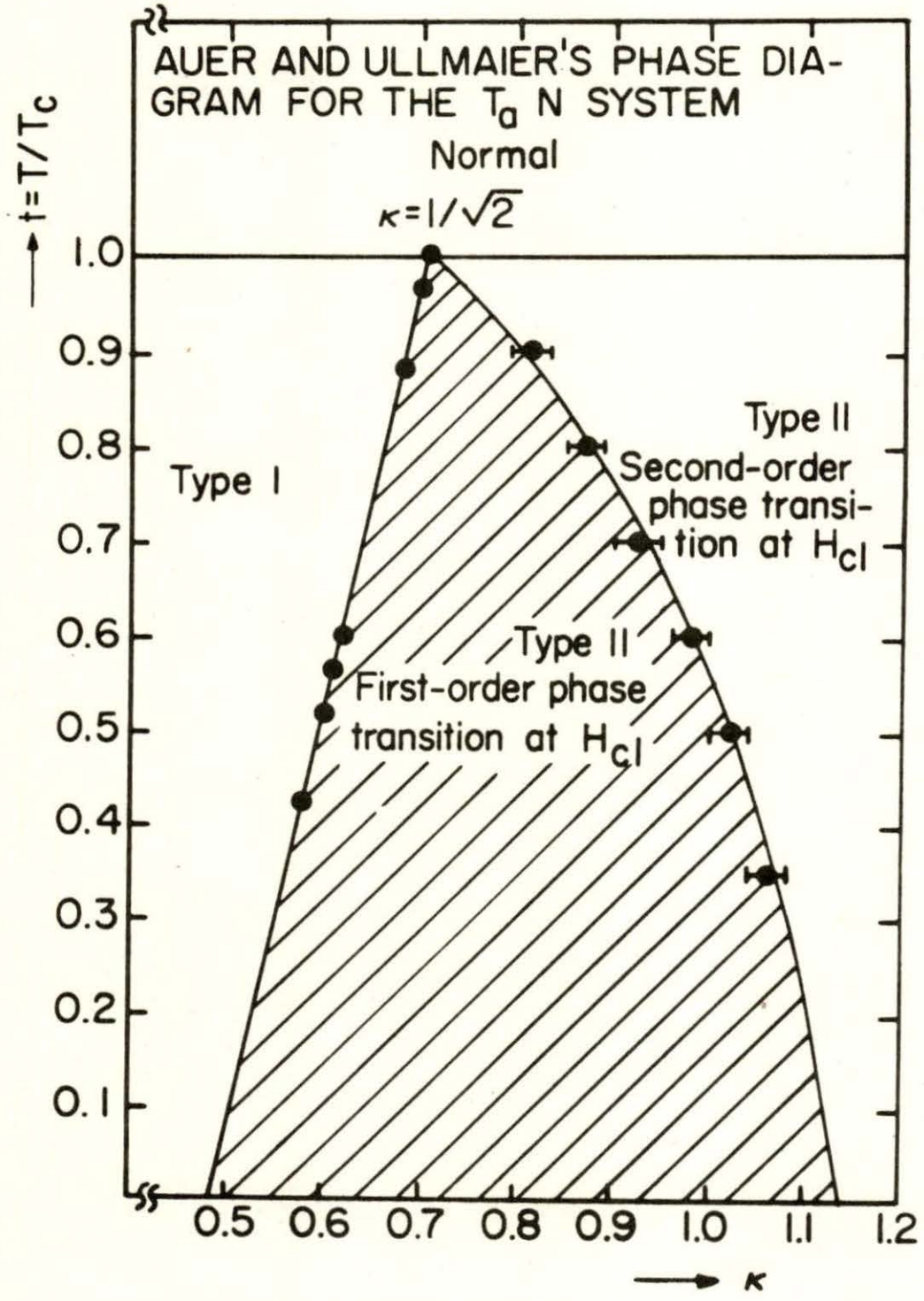

Figure 26. Auer and Ullmaier's phase diagram for the TaN system. See Reference 37.

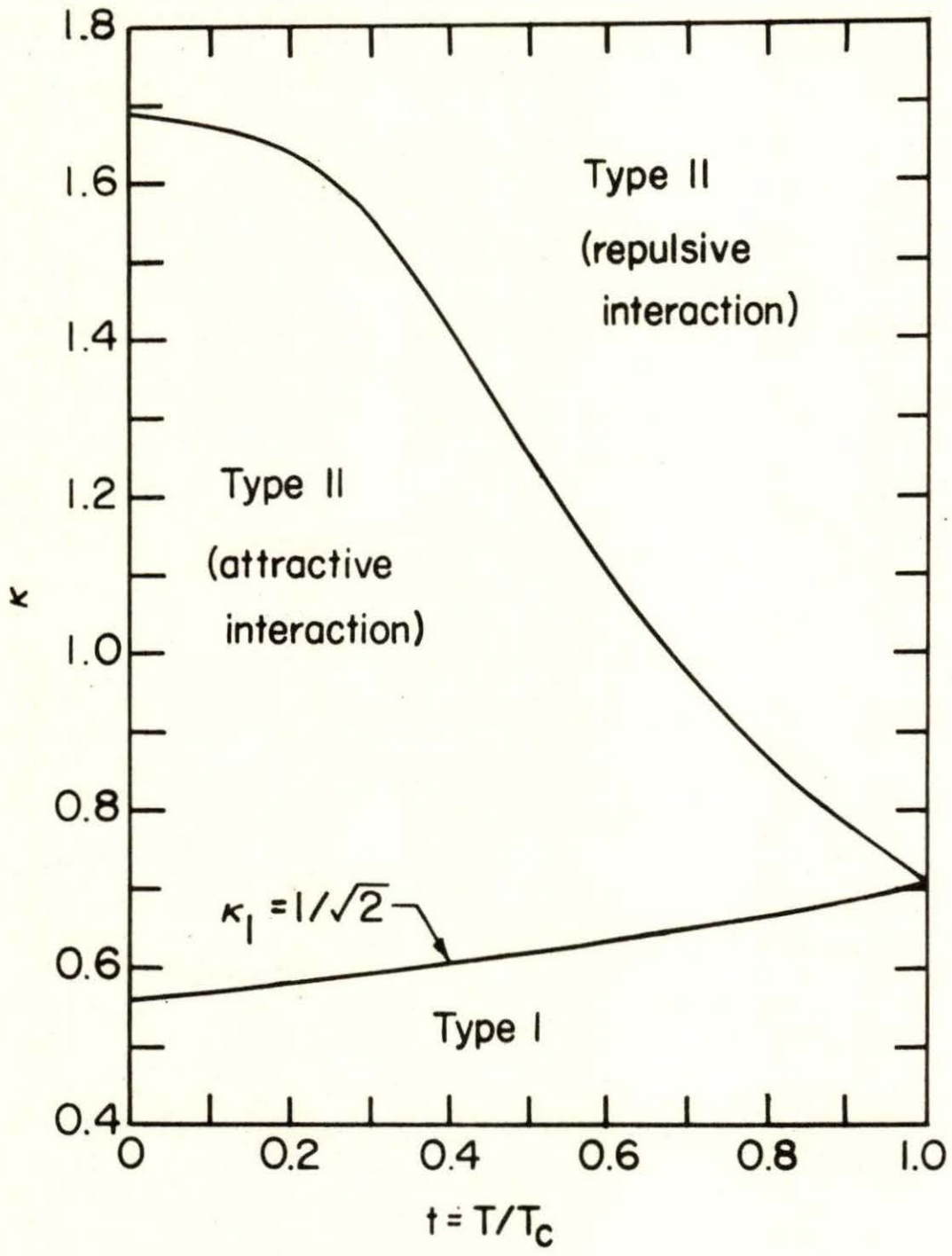

Figure 27. Leung and Jacob's phase diagram for pure metals. See Reference 25.

BIBLIOGRAPHY

1. V. L. Ginzburg and L. D. Landau, Zh. Eksperim. i. Teor. Fiz. 20, 1064 (1950). A complete English translation is available in Men of Physics: L. D. Landau, Vol. 1, edited by D. ter Haar (Pergamon Press, New York, 1965) p. 138.

2. L. P. Gor'kov, Zh. Eksperim. i. Teor. Fiz. 3b, 1918 (1959); Soviet Phys. JETP 9, 1364 (1959).

3. W. Meissner and R. Ochsenfeld, Naturwiss. 21, 787 (1933).

4. L. V. Shubnikov, V. I. Khotkevich, Yu. D. Shepelev, and Yu. N. Riabinin, Zh. Eksperim. i. Teor. Fiz. 7, 221 (1937); Phys. Z. Sowjet. 10, 165 (1936).

5. J. Bardeen, L. N. Cooper, and J. R. Schrieffer, Phys. Rev. 108, 1175 (1957).

6. A. A. Abrikosov, Zh. Eksperim. i. Teor. Fiz. 32, 1442 (1957); Soviet Physics JETP 5, 1174 (1957).

7. B. B. Goodman, Phys. Letters 12, 6 (1964).

8. T. McConville and B. Serin, Rev. Mod. Phys. 36, 112 (1964).

9. T. McConville and B. Serin, Phys. Rev. Letters 13, 365 (1964).

10. T. McConville and B. Serin, Phys. Rev. 140, A1169 (1965).

11. B. Serin, Phys. Letters 16, 112 (1965).

12. U. Krägeloh, Phys. Letters 28A, 657 (1969).

13. U. Krägeloh, Phys. Status Solidi 42, 559 (1970).

14. H. Träuble and U. Essmann, Phys. Status Solidi 20, 95 (1967).

15. G. Eilenberger and H. Büttner, Z. Physik 224, 335 (1969).

16. R. M. Cleary, Phys. Rev. Letters 24, 940 (1970).

17. L. Kramer, Phys. Rev. B 3, 3821 (1971).

18. J. Halbritter, Z. Physik 243, 201 (1971).

19. A. E. Jacobs, Phys. Rev. Letters 26, 629 (1971).

20. K. Dichtel, Phys. Letters 35A, 285 (1971).

21. A. E. Jacobs, Phys. Rev. B 4, 3016 (1971).

22. A. E. Jacobs, Phys. Rev. B 4, 3022 (1971).

23. A. E. Jacobs, Phys. Rev. B 4, 3029 (1971).

24. E. H. Brandt, Phys. Letters 39A, 193 (1972).

25. M. C. Leung and A. E. Jacobs, Thirteenth International Conference on Low Temperature Physics, Boulder, Colorado, 1972.

26. H. Träuble and U. Essmann, Phys. Status Solidi 18, 813 (1966).

27. U. Essmann and H. Träuble, Phys. Letters 24A, 526 (1967).

28. H. Träuble and U. Essmann, Phys. Status Solidi 25, 373 (1968).

29. U. Essmann, Physica 55, 83 (1971).

30. U. Essmann, Phys. Letters 41A, 477 (1972).

31. D. Cribier, B. Jacrot, L. M. Rao, and B. Farmoux, Phys. Letters (Netherlands) 9, 106 (1964); Progress in Low Temperature Physics, Vol. V, edited by C. J. Garten (North Holland Publ. Co., Amsterdam, 1967) p. 161.

32. J. Schelten, H. Ullmaier, and W. Schmatz, Phys. Status Solidi (b) 48, 619 (1971).

33. J. Schelten, H. Ullmaier, and G. Lippman, Z. Physik 253, 219 (1972).

34. D. R. Aston, L. W. Dubeck, and F. W. Rothwarf, Phys. Rev. B 3, 2231 (1971).

35. U. Kumpf, Phys. Status Solidi (b) 44, 829 (1971).

36. D. K. Finnemore, J. R. Clem, and T. F. Stromberg, Phys. Rev. B 6, 1056 (1972).

37. J. Auer and H. Ullmaier, Phys. Rev. B 7, 136 (1973).

38. A. Seeger, Comments on Solid State Physics 3, 97 (1970).

39. S. T. Sekula and R. H. Kernohan, Phys. Rev. B 5, 904 (1972).

40. Ray Radebaugh and P. H. Keesom, Phys. Rev. 149, 209 (1966).

41. O. N. Carlson, F. A. Schmidt, and D. G. Alexander, Metallurgical Transactions 3, 1249 (1972).

42. E. C. Stoner, Phil. Mag. 36, 803 (1945).

43. A. L. Fetter and P. C. Hohenberg, Superconductivity, Vol. 2, edited by R. D. Parks (Marcel Dekker, Inc., New York, 1969) p. 844.

44. B. Lishke and W. Rodewald, Phys. Letters 39A, 321 (1972).

45. E. Helfand and N. R. Werthamer, Phys. Rev. 147, 288 (1966).

46. A. L. Fetter and P. C. Hohenberg, Phys. Rev. 159, 330 (1967).

47. K. Maki, Physics 1, 21 (1964).

48. B. B. Goodman, IBM J. Res. Develop. 6, 63 (1962).

49. G. K. White and S. B. Woods, Can. J. Phys. 35, 892 (1957).

ACKNOWLEDGEMENTS

The author wishes to thank Dr. D. K. Finnemore for his continuing interest and advice in all aspects of this work.

She also wishes to express her appreciation to Mr. F. A. Schmidt for preparing the sample, Mr. J. E. Ostenson for measuring the resistivity ratio and transition temperature, Mr. O. D. McMasters for determining the orientation of the crystals, and Mr. H. K. Baker for electropolishing the sample.

The author is extremely grateful to her husband Michael for his boundless patience and constant encouragement throughout the course of this work, and also for typing the manuscript.

APPENDIX I: GR-251 THERMOMETRY FIT COEFFICIENTS

Range of Validity	Coefficients
0.948-4.299 K	R_o = 5641.60 Ω
	A(0) = -5.3784149E-02
	A(1) = -4.0032365E-01
	A(2) = 1.0702643E-02
	A(3) = -5.0413239E-02
	A(4) = -2.7985169E-02
	A(5) = -6.1945020E-03
	A(6) = 6.7135290E-04
	A(7) = 3.2917364E-04
3.919-9.302 K	R_o = 406.80 Ω
	A(0) = 1.3669533E 00
	A(1) = -6.4326666E-01
	A(2) = 4.2633833E-01
	A(3) = 8.3096200E-01
	A(4) = -1.3324000E-03
	A(5) = -1.2395696E 00
	A(6) = -1.1217528E 00
	A(7) = -3.0779152E-01

APPENDIX II: SUMMARY OF RESULTS

Run	T(K)	$t=T/T_c$	H_c(Oe)	H_{c2}(Oe)	κ_1	κ_2	H_{kink}(Oe)	$-4\pi M_{kink}$(G)	B_o(G)	d_o(Å)
18	1.22	0.225	1390.7	2450	1.246	1.89	1243	647	596	2000
23	1.93	0.355	1261.0	2101	1.178	1.66	1135	587	548	2090
20	3.08	0.567	946.77	1454.2	1.086	1.38	856.0	467.3	388.7	2480
19	3.81	0.702	693.56	992.2	1.012	1.23	629.0	393.0	236.0	3180
21	4.20	0.773	537.51	742.0	0.976	1.15	493.2	305.0	188.2	3560
16	4.42	0.814	450.79	602.5	0.945	1.10	412.0	265.6	146.4	4040
17	4.54	0.836	402.85	530.1	0.930	1.06	369.4	239.2	130.2	4280
11	4.61	0.849	374.07	490	0.926	1.06	342.3	228.0	114.3	4570
12	5.11	0.941	163.67	198.9	0.859	0.91	151.1	108.8	42.3	7520
14	5.19	0.956	132.95	160.8	0.855	0.90	123.3	87.9	35.4	8220
25	5.20	0.958	129.23	155.7	0.852	0.88	120.2	86.3	33.9	8400
26*	4.18	0.770	540.40	751.3	0.983	1.15	494.3	298.0	196.3	3490

*Run 26 data were taken on the reduced sample.